Liebig-aged (*c.* 1640 Ma) magmatism and metamorphism in *c.* 1760 Ma crust in the Warumpi and southern Aileron Province, central Australia: a case for revising the tectonic framework of Proterozoic Australia

Thesis submitted in accordance with the requirements of the University of Adelaide for an Honours Degree in Geology

Courtney Elizabeth Fields

November 2012

THE UNIVERSITY of ADELAIDE

LIEBIG-AGED (*c.* 1640 Ma) MAGMATISM AND METAMORPHISM IN *c.* 1760 Ma CRUST IN THE WARUMPI AND SOUTHERN AILERON PROVINCE, CENTRAL AUSTRALIA: A CASE FOR REVISING THE TECTONIC FRAMEWORK OF PROTEROZOIC AUSTRALIA

LIEBIG-AGED TECTONISM IN THE WARUMPI & AILERON PROVINCES

1 ABSTRACT

The southern margin of the North Australian Craton (NAC) has been suggested to represent a long-lived (*c.* 1860 to 1600 Ma) active margin that preserves a cryptic record of the growth and assembly of the Australian continent. The Warumpi Province is juxtaposed against the southern Aileron Province, and has been interpreted as exotic to the NAC, though the timing of collision between the Warumpi Province and the southern Aileron Province is contentious. U-Pb zircon and monazite LA-ICP-MS geochronology from granulite facies metapelites and granitic gneisses along the southern margin of the Aileron Province and northern margin of the Warumpi Province, has shown it is characterised by *c.* 1780-1740 Ma magmatic rocks and c. 1640-1615 Ma magmatic and metamorphic rocks. The evidence for these events is preserved in kilometre-scale migmatitic boudins and low-strain zones enveloped by pervasive E-W trending higher strain belts. The overprinting high strain fabrics are Grenvillian age and constrained to *c*. 1175-1070 Ma. Phase equilibria modelling on a garnet-sillimanite-cordierite metapelite dated at *c.*1616 Ma, from a low-strain domain within the southern Aileron Province, indicates that peak metamorphic conditions were ~7-8 kbar and between 740-900 °C, and were associated with a down-pressure or decompressional *P-T* history. A metamorphic monazite age of *c.*1620 Ma was also preserved in a granitic gneiss located in an older, low-strain domain. The presence of the *c.* 1760 Ma and *c.* 1640 Ma timelines in both the Warumpi and Aileron Provinces calls into question the proposed exotic nature of the Warumpi Province. A speculative interpretation is that the Liebig-aged metamorphism and magmatism, seemingly associated with relatively shallow orientated, low strain fabrics, represents a period of extension rather than collision.

KEYWORDS

Proterozoic Australia, Aileron Province, Warumpi Province, southern Arunta region, North Australian Craton, U-Pb zircon geochronology, U-Pb monazite geochronology

TABLE OF CONTENTS

2 LIST OF FIGURES & TABLES

3 INTRODUCTION

The southern margin of the North Australian Craton (NAC) is a key area of Proterozoic Australia as it has been suggested to represent a long-lived (from *c.* 1860 to 1600 Ma) active margin (Collins & Shaw 1995, Betts *et al.* 2002, Giles *et al.* 2004, Scrimgeour *et al.* 2005b, Betts & Giles 2006, Wade *et al.* 2006, Betts *et al.* 2008, Cawood & Korsch 2008) that preserves a cryptic record of the growth and assembly of the Australian continent. The southern NAC comprises the southern part of the Aileron Province of the Arunta region, and the Warumpi Province (Figure 1). The Warumpi Province is juxtaposed immediately against the southern Aileron Province, and has been interpreted to be a terrain that was exotic to the NAC (Scrimgeour *et al.* 2005b), though the timing of its docking with the Aileron Province/NAC has proven contentious (Scrimgeour *et al.* 2005b, Morrissey *et al.* 2011, Wong 2011). Unravelling the Proterozoic history of the southern NAC and the adjacent Warumpi Province is challenging due to the large number—at least six—of regional-scale deformation events that have reworked the region. Moreover, despite the importance of this region to models of continental growth or assembly, there have been relatively few studies that have specifically targeted the age of magmatic rocks, differing structural fabric domains and events in the Warumpi and southern Aileron Provinces. Such fundamental data is critical for underpinning larger-scale tectonic models.

This study focusses on rocks of the southernmost Aileron Province and northern Warumpi Province. These regions extensively outcrop in an EW-trending belt over a distance of approximately 200 km between the Redbank Shear Zone, Desert Bore Shear Zone and Neoproterozoic sedimentary rocks of the MacDonnell and Chewings Ranges (Figure 2).

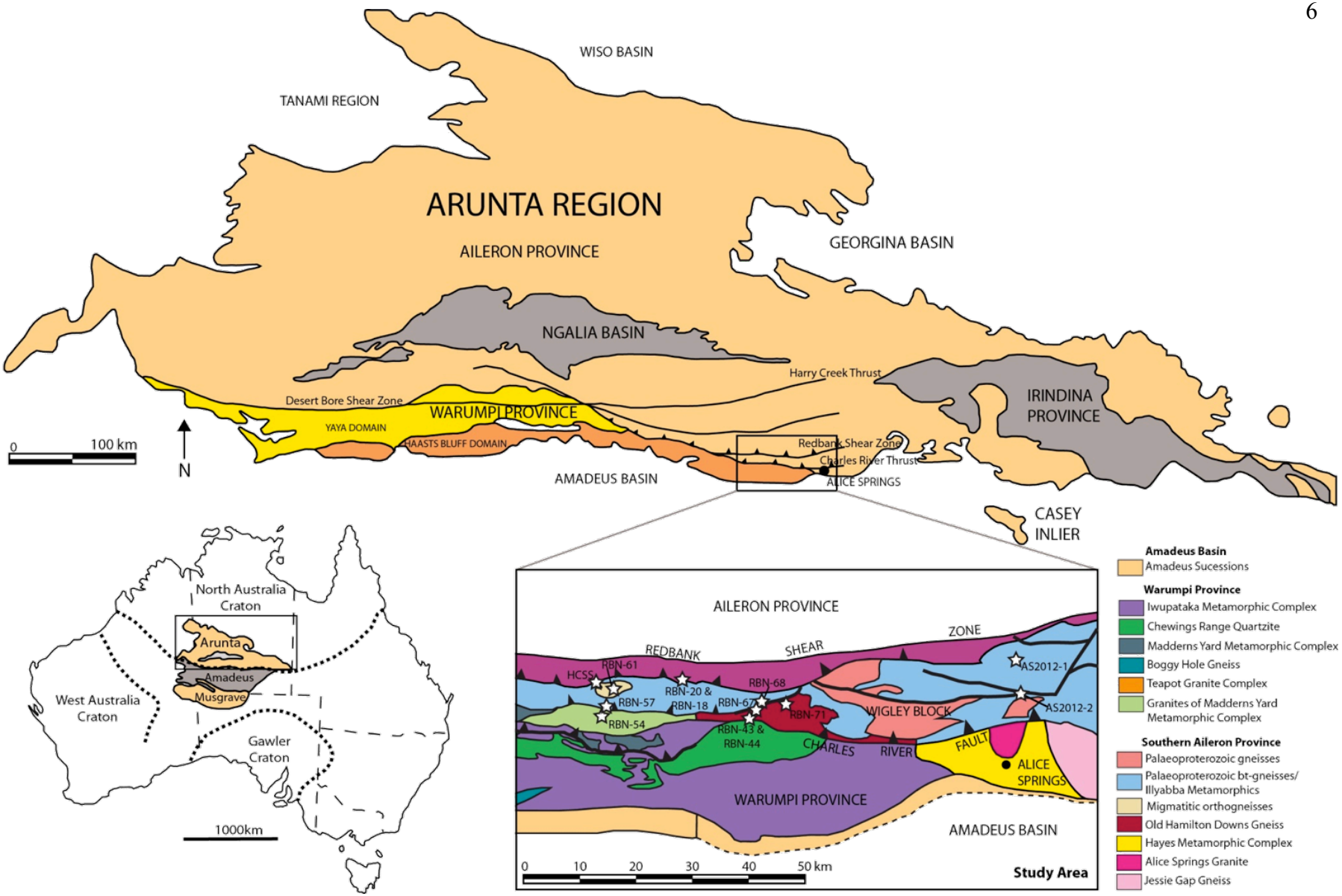

Figure 1: Simplified geological map of study area and sample locations with respect to Arunta region, central Australia (adapted from Scrimgeour *et al.*2005a, Wong 2011). This study is focused on the southern margin of the Aileron Province and the Warumpi Province to the south. The boundary between the Warumpi and Aileron Provinces in the study area is interpreted to be the Charles River Thrust. Coupled with the Redbank and Desert Bore Shear Zones, these major faults represent the interpreted Central Australian Suture. The inset solid geology map of the study area displays the spatial distribution of sample locations either side of the Aileron-Warumpi boundary.

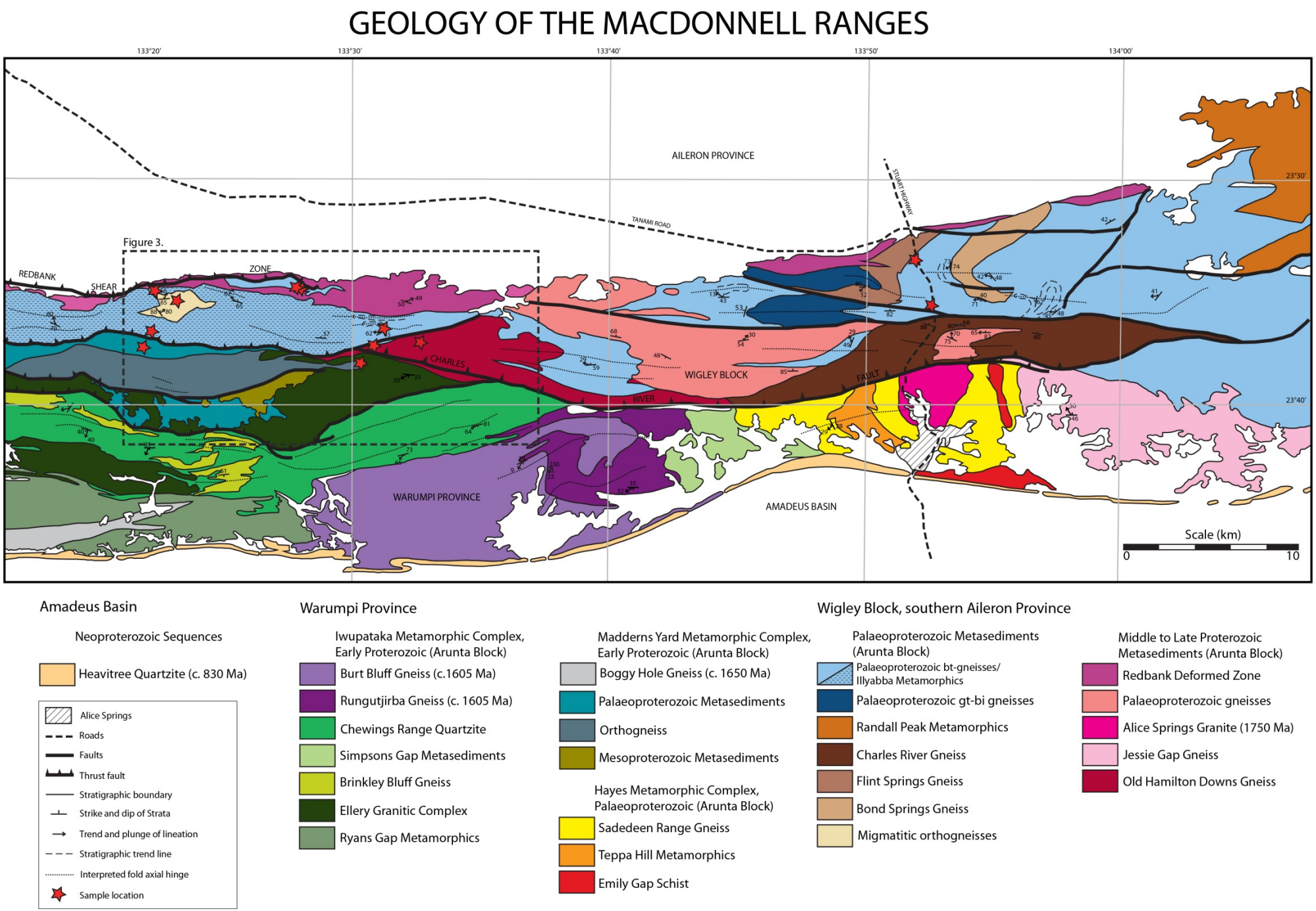

Figure 2: Geological map of the primary study region demonstrating the distribution of major lithologies and geological structures within southern Aileron Province and Warumpi Province (adapted from Wong, 2011). An area of significant interest (dashed outline) is highlighted and expanded upon in Figure 3.

The specific study area is located approximately 30 km NW of Alice Springs (Figure 1) and comprises high-grade, transitional amphibolite–granulite facies rocks that are considered part of the Warumpi Province in the south and the southernmost Aileron Province (Scrimgeour *et al.* 2005b). There is relatively little geochronological data for basement rocks south of the Redbank Shear Zone (Collins *et al.* 1995, Biermeier *et al.* 2003, Scrimgeour *et al.* 2005b, Morrissey *et al.* 2011, Wong 2011).

The purpose of this study is to obtain U-Pb geochronological data for a range of rocks and modern stream sediments from the Warumpi and southernmost Aileron Province, as well as constrain the metamorphic conditions of the crust for a key event timeline, with the aim of establishing a robust framework for the tectonic history of the region. The data collected in this study has direct application to the larger question of the tectonic and geodynamic significance of key event timelines in Proterozoic Australia.

4 GEOLOGICAL SETTING

4.1 Regional Geology

The geology of the Arunta region in central Australia encompasses an ~ 200,000 km^2 region of Palaeoproterozoic to Palaeozoic aged, magmatic, and intermediate to high grade metamorphic rocks juxtaposed against Neoproterozoic to Phanerozoic sedimentary basins (Haines *et al.* 2001). The southern margin of the NAC (i.e. southernmost Aileron Province) is interpreted to record a prolonged history of sedimentation, arc-related magmatism, episodic orogenesis and accretionary tectonism, in conjunction with subduction related processes between *c.*1860–1600 Ma (Zhao 1994, Collins & Shaw 1995, Scott *et al.* 2000, Giles *et al.* 2002, 2004, Hoatson *et al.* 2005, Maidment *et al.* 2005, Scrimgeour *et al.* 2005b, Betts & Giles 2006, Wade *et al.* 2006, Betts *et al.* 2008, Cawood & Korsch 2008, Claoue-Long *et al.* 2008).

The Arunta region has historically been subdivided into three distinct provinces (Figure 1) governed by differing protolith ages and histories (Scrimgeour *et al.* 2005b). The provinces are the Aileron Province, Warumpi Province, and Irindina Province. The Irindina Province is dominated by Neoproterozoic to Cambrian aged rocks and it is not discussed further here (Hand *et al.* 1999, Mawby *et al.* 1999).

Event timelines that have shaped the Palaeo- and Meso- Proterozoic geology of the Arunta region are detailed in Table 1 (Scrimgeour 2003a, Morrissey *et al.* 2011), spanning the Stafford Event (*c.* 1810-1800 Ma; Claoué-Long & Edgoose 2008) through to the most recent, the Alice Springs Orogeny (*c.* 400-300 Ma). This resulted in the exhumation of the Arunta region from beneath the formerly contiguous Centralian Superbasin (Haines *et al.* 2001), with the greatest amount of exhumation accommodated by the north-dipping, crustal-scale Redbank Shear Zone (Teyssier 1985, Lambeck *et al.* 1988, Goleby *et al.* 1989, Shaw *et al.* 1992, Korsch *et al.* 1998, Sandiford & Hand 1998, Flöttmann & Hand 1999).

The majority of the Proterozoic events summarised in Table 1 have been linked to larger-scale tectonic processes relating to continental assembly (*e.g.* Betts & Giles, 2006; Wade *et al* 2006; Giles *et al* 2004; Myers *et al* 1996; Payne *et al* 2009; Scrimgeour *et al* 2005). Intriguingly, the majority of Proterozoic events recorded in the Arunta region are inferred as collisional/compressional but are characterised by metamorphic rocks indicative of low-pressure/high-temperature metamorphism (e.g. Offe & Shaw 1983; Norman & Clarke 1990; Dirks & Wilson 1990; Clarke & Powell 1991 (Reynolds); Collins & Vernon 1991; Dirks *et al.* 1991; Goscombe 1992 (Strangways); Buick & Cartwright 1995 (Reynolds/Chewings); Collins & Shaw 1995; Warren & Shaw 1995; Vry *et al*. 1996 (Reynolds/Chewings); Greenfield *et al.* 1998 (Stafford); Hand & Buick 2001; Rubatto *et al*. 2001 (Reynolds/Chewings); Biermeier *et al.* 2003; Scrimgeour 2003; White *et al.* 2003

Table 1: Summary of major tectonic events that have created and shaped the Arunta region.

EVENT NAME	AGE (Ma)	REGIONAL DISTRIBUTION	MAGMATISM	METAMORPHIC CHARACTER	DEFORMATION
Stafford Event	**1810-1800** (Claoue Long & Hoatston, 2005)	Central and northen Aileron Province	Granitic and mafic	Localised low P, high T up to granulite grade (maximum *P-T* 850 °C & 3 kbar)	Low strain predominantly thermal event
Yambah Event	**1780-1760** (Claoue Long & Hoatston, 2005)	Central and southern Aileron Province	Granitic and mafic	Low-medium P, high T up to granulite grade (maximum *P-T* poorly known but possible > 800 °C & 8 kbar)	Deformational character poorly known but probably compressional
Inkamulla Igneous Event	**1760-1740** Scrimgeour *et al.* 2003	Southeastern Aileron Province	Granitic and mafic - includes apparent arc-related and a-type magmatism	Metamorphic character not known	Deformational character unknown
Early Strangways Orogeny	**1730-1715** Claoue Long *et al.* 2008)	Southeastern and southern Aileron Province	Minor felsic magmatism	Low-medium P, high T up to granulite grade (maximum *P-T* poorly known but possible > 800°C & 8 kbar)	Regional high-grade deformation (assumed to be compressional)
Late Strangways Orogeny	**1700-1670** Claoue-Long *et al.* 2008; Hand unpublished)	Southeastern and southern Aileron Province	Abundant mafic dykes	Medium *P-T* up to granulite grade (maximum *P-T* 800 °C & 7 kbar)	Regional -scale mylonites and large scale sheath folds associated with east-directed extension that rework Early Strangways Orogeny structures
Argilke Igneous Event	**1690-1670**	Southern Warumpi Province (Scrimgeour et al 2005)	Volumetrically significant predominantly felsic magmatism	Metamorphic character poorly known, but up to upper amphibolite grade	Deformational character unknown
Leibig Orogeny	**1640-1630**	Central Warumpi Province and southern Aileron Province (Scrimgeour *et al.*, 2005; Wong 2011)	Volumetrically significant predominantly felsic magmatism, but also mafic to ultramafic magmatism	Regional metamorphic grade poorly known, but locally up to high *P-T* granulite (maximum *P-T* 900 °C & 9 kbar	Deformational character unknown
Ormiston Event	**1620-1600**	Southern Warumpi Province (Scrimgeour *et al*. 2005)	Volumetrically significant predominantly felsic magmatism, with a comparatively juvenile character	Metamorphic character unknown	Deformational character unknown, but associated with sedimentation
Chewings Orogeny	**1600-1550** (Claoué-Long et al. 2008; Hand & Buick, 2001)	Central Warumpi Province and southern and central Aileron Province (Hand & Buick; Wong, 2011)	Minor felsic magmatism in high-grade metamorphics in the Central Aileron Province, volumetrically significant felsic magmatism in the Central western Aileron Province	Regional LPHT metamorphism up to granulite grade (maximum PT 850 °C and 6 kbar)	Compressional deformation with regions associated with top to the S transport
TeapotThermal Event	**1160-1130** (Morrissey et al., 2011)	Waumpi Province and southern Aileron Province	Felsic to mafic and ultramafic	Regional metamorphism up to upper amphibolite-transitional granulite (maximum *P-T* 800 °C and 6 kbar)	Compressional with regional-scale E-W trending isoclinal folding and south up shear systems

(Stafford); Maidment *et al.* 2005; Scrimgeour *et al*. 2005a; Claoue-Long *et al.* 2008b (Strangways); Morrissey *et al.* 2011). This style of metamorphism indicates an elevated geothermal gradient and is therefore, more akin to an extensional (or high heat flow regime), rather than a collisional one. The most blatant exception is the interpretation of high-pressures (approximately 9–10 kbar) for metamorphism during the ~1640 Ma Liebig Orogeny (Scrimgeour *et al.* 2005).

4.2 Study Area

The study area, which is located between the Redbank Shear Zone and the Chewings and MacDonnell Ranges (Figure 2), comprises rocks of the Warumpi Province and southernmost Aileron Province. The boundary between the Warumpi and Aileron Province in the study area is interpreted to be the Charles River Thrust (Northern Territory Geological Survey 2012; Figure 2), with the Redbank and Desert Bore Shear Zones delineating the boundary progressively further to the west (Figure 1).

Lithological units in the study area (Figure 2) comprise the Illyabba Metamorphics (southernmost Aileron Province) and the Madderns Yard Complex (Warumpi Province). The Illyabba Metamorphics are mainly migmatitic felsic gneisses, with homogeneous quartzo-feldspathic orthogneiss, minor quartzite and metapelite and minor mafic granulite and unnamed megacrystic orthogneiss (Pgc). The Illyabba Metamorphics are interpreted to correlate with the adjacent unnamed Palaeoproterozoic gneiss units to the east (Offe & Shaw 1983, Warren & Shaw 1995). The Madderns Yard Complex in the study area comprises unnamed migmatitic quartzofeldspathic gneiss, biotite-rich migmatite and minor metasediments and amphibolite (all *Pmo*). The Madderns Yard Metamorphic Complex is overlain by the 1620-1610 Ma Iwupataka Metamorphic Complex, which consists of metamorphosed (but not migmatised) metasediments, volcanics and granites. It includes the

Chewings Range Quartzite and Simpsons Gap Metasediments, which are intruded by the 1605 Ma Burt Bluff Gneiss and mafic to ultramafic Cummings Leucogabbro, respectively (Warren & Shaw 1995). Existing geochronological constraints from the region (Offe & Shaw 1983, Collins & Shaw 1995, Collins *et al.* 1995, Warren & Shaw 1995, Zhao & Bennett 1995, Biermeier *et al.* 2003, Claoué-Long & Hoatson 2005, Scrimgeour *et al.* 2005b, Carson *et al.* 2009, Morrissey *et al.* 2011, Wong 2011) provide only a rudimentary understanding of the geological event framework of the region.

Of the events summarised in Table 1, evidence for the Yambah, Inkamulla, Liebig, Ormiston Igneous, and Teapot Thermal events are recorded in this EW-belt of outcrop contrary to previous interpretations (e.g Teyssier *et al*. 1988). The Chewings Event does not appear to have affected this region (Morrissey *et al.* 2011), in a recognisably pervasive manner. The Yambah and Inkamulla events are believed to be manifest as magmatism within the Aileron Province part of this EW-belt (Zhao & Bennett 1995, Scrimgeour 2003a). Magmatic and/or metamorphic ages of *c.* 1780 Ma and *c.* 1750 Ma are considered to represent Aileron Province crust (Scrimgeour *et al.* 2005b, Claoue-Long *et al.* 2008).

The Liebig Orogeny is proposed to be responsible for the collisional docking of the exotic Warumpi Province with the southern Aileron Province (NAC) at *c.* 1640 Ma (Scrimgeour *et al.* 2005b). Constraint on the timing of this event is largely provided by the study of Scrimgeour *et al.* (2005b). However, age constraints are also provided by Collins & Shaw (1995) Scrimgeour (2003b) and Claoué-Long & Hoatson (2005), so that the Liebig Orogeny is currently believed to span 1640–1630 Ma. The Liebig Orogeny is proposed to involve ocean closure, with the south-dipping suture (Selway *et al.* 2009) being represented by the Desert Bore Shear Zone, Redbank Shear Zone and Charles River Thrust, respectively, from west to east (Scrimgeour *et al.* 2005b). Syn-tectonic magmatism occurred during the Liebig

Orogeny (Scrimgeour *et al.* 2005b), however, the deformational framework is unknown. Curiously, mafic-ultramafic intrusions of the Andrew Young Complex were emplaced into the southern Aileron Province during the Liebig Orogeny (Claoué-Long & Hoatson 2005), casting doubt on the inferred collisional-accretion tectonic interpretation. Furthermore, Wong (2011) found evidence for *c.* 1640 Ma magmatism in crustal rocks attributed to the Aileron Province, raising questions about the exotic nature of rocks containing Liebig-aged magmatic rocks. Given the ambiguity surrounding the Liebig Orogeny, it is important to constrain the age of fabrics that can be attributed to this event, as their orientation may offer insight into the tectonic setting at the time.

East-west–trending high-strain zones with a (typically) steeply north-dipping fabric control the outcrop pattern in the Warumpi and southernmost Aileron Province (Figure 3). Historically these steep zones of reworking were considered to be the product of the compressional Chewings Event (e.g. Teyssier *et al.* 1988; Collins & Shaw 1995). However, these zones have been demonstrated to be the product of reworking during the Grenvillian time period (Wong 2011), coincident with the Musgrave Orogeny to the south of the Amadeus Basin (Smithies *et al.* 2011). Grenvillian-aged reworking does not appear to continue north of the Redbank Shear Zone (Lawson-Wyatt 2012).

4.3 Rock Types & Sample Locations

The field work for this study was aimed at sampling relative low-strain domains enclosed by regional upright shear zones and folds of interpreted Grenvillian age, for the purpose of providing tight spatial, temporal and tectonic constraints to gain insight into the pre-Grenvillian history (Figure 3). The locations and detailed descriptions of the samples analysed are provided in Table 2.

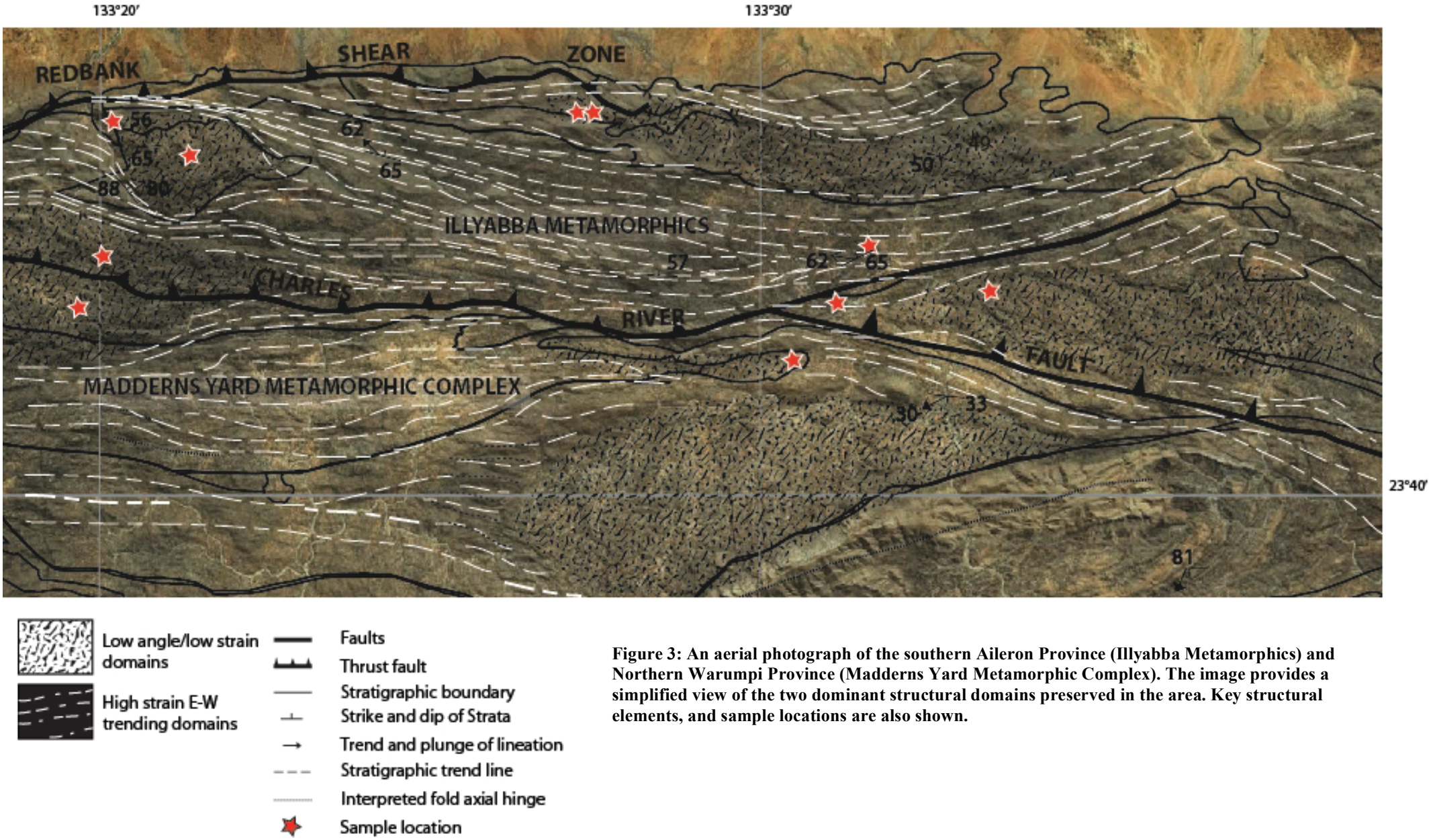

Figure 3: An aerial photograph of the southern Aileron Province (Illyabba Metamorphics) and Northern Warumpi Province (Madderns Yard Metamorphic Complex). The image provides a simplified view of the two dominant structural domains preserved in the area. Key structural elements, and sample locations are also shown.

Table 2: Summary of samples analysed in this study; including grid reference, lithological unit, rock type and field descriptions.

SAMPLE	EASTING (m) Zone 53 K	SOUTHING (m) Zone 53 K	PROVINCE	UNIT	LITHOLOGY	STRUCTURAL SETTING	ANALYSES
AS2012-1	384435	7394616	Aileron	Unnamed Palaeoproterozoic gneiss (Illyabba Metamorphics)	Migmatitic granitic gneiss	Sample located within an outcrop with an intense fabric that is folded by upright E-W trending folds.	Zircon U-Pb LA-ICP-MS
AS2012-2	385668	7389949	Aileron	Unnamed Palaeoproterozoic gneiss (Illyabba Metamorphics)	Migmatitic orthogneiss	Sample is folded into open gently west plunging folds. The fabric envelope of the migmatitic fabric appears low angle.	Zircon U-Pb LA-ICP-MS
RBN-18	342229	7391261	Aileron	Unnamed Palaeoproterozoic gneiss (Illyabba Metamorphics)	Sill-cd-gt-bi metapelitic granulite	Large area of outcropping metasediments, gt+sill metapelites as well as more psammitic outcrops. RBN-18 is a sill-cd-gt-bi metapelite with a S-E trending fabric being truncated by E-W trending fabric about 20 m to the north; sample located in a targeted low-strain region.	Zircon U-Pb LA-ICP-MS Monazite U-Pb LA-ICP-MS P-T Pseudosection Garnet Mapping
RBN-20	342330	7391309	Aileron	Unnamed Palaeoproterozoic gneiss (Illyabba Metamorphics)	Folded porphyroclastic granite	This granite outcrop has three generations of leucosomes; 1st generation are folded, 2nd generation are partially folded, and the latest generation are cross-cutting the folded fabric. This sample was collected from a targeted low-strain region.	Zircon U-Pb LA-ICP-MS
RBN-43	347748	7383931	Warumpi	Madderns Yard Metamorphic Complex	Qtz-ksp-bi pegmatite with seam of euhedral garnet	This sample is from a wide, coarse-grained pegmatite with an undulating margin that quite clearly cross-cuts the gneissic fabric. Seams of euhedral garnet appear rarely throughout the pegmatite.	Monazite U-Pb LA-ICP-MS
RBN-44	347748	7383931	Warumpi	Madderns Yard Metamorphic Complex	Ksp-rich porphyroclastic granitic gneiss	Highly strained granitic gneiss, to an almost L-tectonite. South-up kinematics on a south-dipping fabric.	Zircon U-Pb LA-ICP-MS Monazite U-Pb LA-ICP-MS

RBN-54	328349	7386229	Warumpi	Unnamed Palaeoproterozoic gneiss (*Pmo*) (Madderns Yard Metamorphic Complex)	Bi- gneiss	Fabric is weak, within the Pmo unit. In close proximity (~1 metre) to a mylonite, this has a fabric 097/48°N. Lineation of mylonite is 47→003. Sample was collected from a targeted low-strain region.	Zircon U-Pb LA-ICP-MS Monazite U-Pb LA-ICP-MS
RBN-57	329072	7387398	Aileron	Unnamed Palaeoproterozoic gneiss (Illyabba Metamorphics)	Megacrystic ksp-rich	Outcrop is weakly foliated, granitic gneiss with a leucosome cross-cutting it. Gneissic fabric is shallowly dipping. Sample was collected from a targeted low-strain region.	Zircon U-Pb LA-ICP-MS
RBN-61	332201	7390342	Aileron	Unnamed Palaeoproterozoic migmatitic orthogneiss (*Pgc*)	Megacrystic migmatitic orthogneiss	Sample is taken from within a relative low strain region, i.e. a kilometre scale boudin. Weakly to moderately foliated granitic orthogneiss; fabric is lower strain than fabrics observed within the E-W Grenvillian overprinting zones.	Zircon U-Pb LA-ICP-MS Monazite U-Pb LA-ICP-MS
RBN-67	348649	7385840	Aileron	Old Hamilton Downs Gneiss	Quartzofeldspathic gneiss	Medium-fine grained, with a prominent lineation defined by quartz ribbons and biotite. Sample was targeted within an outcrop of shallowly dipping fabric.	Zircon U-Pb LA-ICP-MS Monazite U-Pb LA-ICP-MS
RBN-68	349485	7387359	Aileron	Unnamed Palaeoproterozoic gneiss; (Illyabba Metamorphics)	Granitic to quartzofeldspathic gneiss	Moderately dipping outcrop, strong to moderate fabric/gneissosity. Coarse magnetite grains or aggregates. Strongly foliated, with some folding preserved.	Zircon U-Pb LA-ICP-MS Monazite U-Pb LA-ICP-MS
RBN-71	352800	7387700	Aileron	Old Hamilton Downs Gneiss	Bi-mt granite/granitic gneiss	Sample located 500 metres south of an approx. 300m wide mylonitic zone running SW-NE. Sample is from a rounded, incongruous outcrop with a weak and fairly indistinct foliation; poorly defined fabric. Sample was collected from a targeted low-strain region.	Zircon U-Pb LA-ICP-MS Monazite U-Pb LA-ICP-MS
HCSS	329851	7390904	N/A	N/A	Alluvium	Modern stream sediments collected at the mouth of Hamilton Creek, immediately south	Zircon U-Pb LA-ICP-MS

of the Redbank Shear Zone.

Samples were collected along roughly north-south transects along creeks which lie at a high angle to the E-W trending Grenvillian-aged belts. In addition, a modern stream sediment sample was collected from the mouth of Hamilton Creek. The drainage basin for Hamilton Creek comprises only outcrop to the north of the Chewings Range (quartzite), implying that stream sediment collected from Hamilton Creek provides an efficient means of characterising the ages of rocks and events in the Illyabba (Aileron Province) and Madderns Yard (Warumpi) Metamorphics.

Two samples, AS2012-1 & -2 were collected from unnamed Palaeoproterozoic gneisses in the eastern Wigley Block, which is a fault-bounded region between the Charles River Fault and Redbank Shear Zone in the southern Aileron Province (Wong 2011).

A region located by the Hamilton Downs Youth Camp, ~35 km to the west of the Stuart Highway was also sampled, within the same structural belt. Here, samples RBN-43 & -44 were collected from the Madderns Yard Metamorphics Complex south of the Aileron-Warumpi boundary within the Warumpi Province; RBN-67 and RBN-71 from the Old Hamilton Downs Gneiss, and RBN-68 from the Illyabba Metamorphics, all in the southern Aileron Province.

A further ~10km to the west, within the same structural belt, RBN-18 & -20 were sampled from the Illyabba Metamorphics of the southern Aileron Province, and more specifically from within an unretrogressed lens between E-W trending assumed Grenvillian aged high-strain zones southeast of Blackhill Dam, known to contain cordierite-bearing metapelites (Warren & Shaw 1995).

Lastly, samples RBN-54, -57 & -61 were sampled a further ~10 km to the west at Hamilton Creek. Sample RBN-61 was sampled from within a kilometre scale, low strained megaboudin, composed of unnamed orthogneiss (*Pgc*) and completely enveloped by Illyabba

Metamorphics with an E-W trending fabric which has an age of *c*. 1140 Ma (Wong 2011, Figure 4). RBN-57 was sampled within the Illyabba Metamorphics, and RBN-54 was again across the Aileron-Warumpi border within the Madderns Yard Metamorphics.

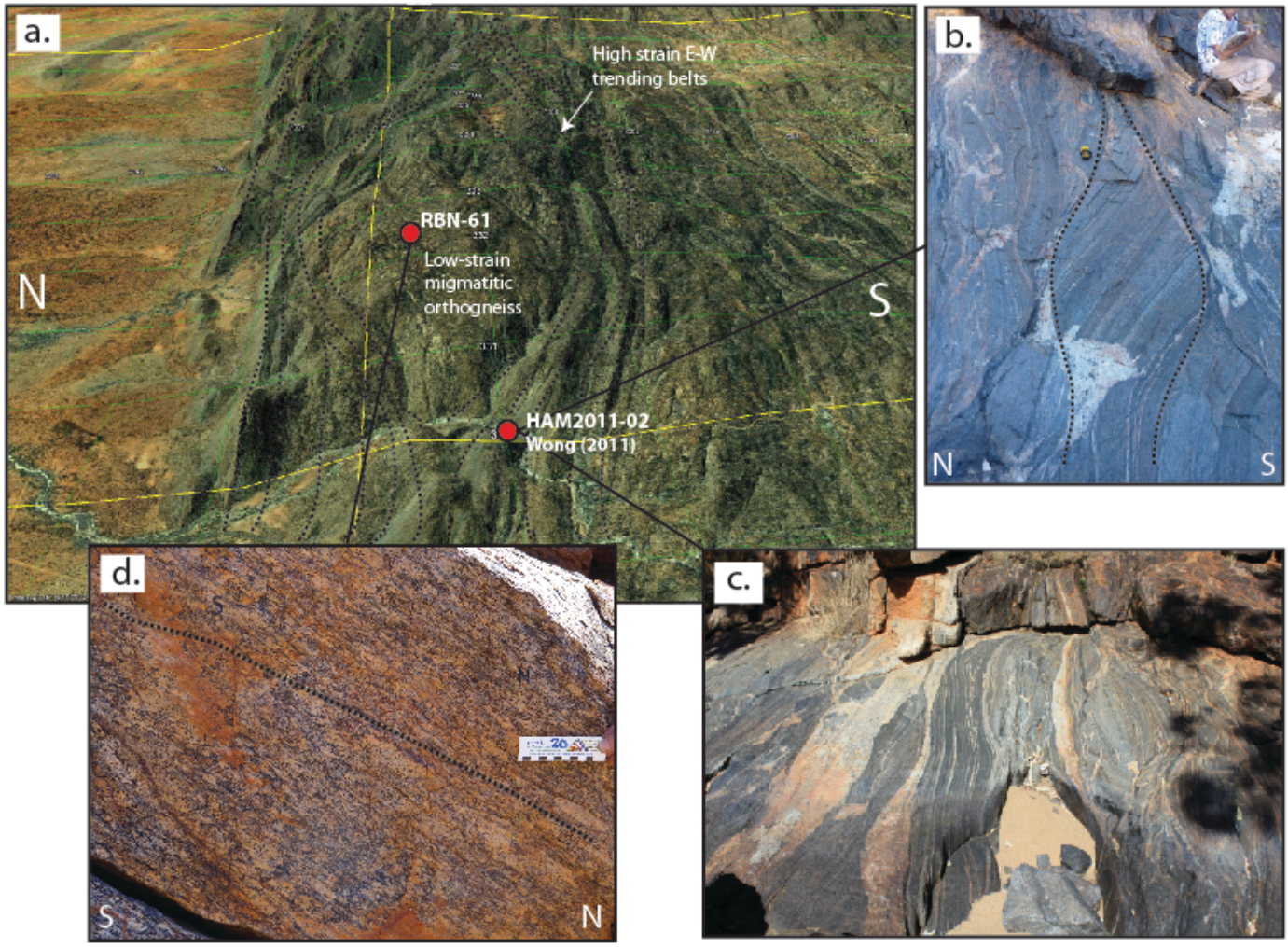

Figure 4: Field photographs showing the two dominant structural domains present in the field area. (a) shows an oblique aerial view of the kilometre scale, low strained megaboudin, composed of unnamed orthogneiss (*Pgc*) with the sample location of RBN-61 (low strain) and HAM2011-02 (high strain). The regional orthogneiss boudin, preserving an igneous protolith age of 1741 ± 8 Ma, and a metamorphic age of 1625 ± 7 Ma is completely enveloped by Illyabba Metamorphics with an E-W trending fabric dated at *c*. 1140 Ma (Wong 2011). Due to the angle of the image, a scale bar could not be represented; however the area between the yellow lines is10 km^2 and the area between the green lines is 1 km^2. High-strain fabrics at HAM2011-02 are demonstrated by: (b) large mafic migmatitic boudin that also demonstrates the same kinematics in out-crop scale seen at the region-scale (see Figure 4a); and (c) Mafic migmitised orthogneiss with syn-tectonic felsic pegmatites. Low-strain fabric at RBN-61 (d) shows the megacrystic, migmatitic orthogneiss with a relatively flat-lying foliation. The distance between the sample locations is 2.4 km.

5 ANALYTICAL METHODS

5.1 Elemental X-Ray Mapping

Chemical analyses of minerals and elemental x-ray maps were obtained using a Cameca SX5 Electron Microprobe at the University of Adelaide. Elemental mapping of garnet grains in sample RBN-18 was undertaken using beam conditions of 100 nA and 15 kV. Elements Mg, Ca, Mn, Na and Fe were mapped with wavelength dispersive spectrometers (WDS) and Al, Si, K, Ti, V, Cr and Co were mapped with an energy dispersive spectrometer (EDS).

5.2 Phase Equilibria Modelling

Phase diagram calculations are based on whole-rock compositional data obtained at Amdel Laboratories, Adelaide (see Appendix A). The method follows that of de Capitani & Petrakakis (2010) and a full description of the techniques followed is included in Appendix B.

5.3 Geochronology

Samples were selected for U-Pb monazite and zircon geochronology based on the structural setting of the sample with respect to the kilometre-scale outcrop pattern of boudins (low strain zones potentially preserving older history) and wrapping higher-strain fabrics (see Table 2). Monazite geochronology was used to constrain the age of reworking/metamorphism and was obtained from eight samples (RBN-18, -43, -44, -54, -61, -67, -68 and -71). Zircon geochronology was used to constrain magmatic ages, timing of metamorphic events and the maximum depositional age of metasediments; twelve samples (AS2012-1 & -2, RBN-18, -20, -44, -54, -57, -61, -67, -68, -71 and HCSS) were analysed. Methods follow that of Payne *et al*. (2008) and a full description of the techniques followed is included in Appendix C.

Ages quoted throughout the study are $^{207}Pb/^{206}Pb$ ages as the data contains ages older than *c.* 1000 Ma and all errors stated in data tables and alongside concordia diagrams are at the 1σ level. Concordancy was calculated using the ratio of ($^{206}Pb/^{238}U$) / ($^{207}Pb/^{206}Pb$).

6 RESULTS

6.1 Metamorphic Petrology

The selected sample for metamorphic petrography and pressure-temperature (*P–T*) analysis (phase equilibria modelling) was RBN-18, a weakly foliated metapelite (Figure 5). Sample RBN-18 contains garnet, sillimanite, cordierite, biotite, potassium feldspar and quartz with accessory amounts of ilmenite, magnetite, zircon and monazite. Garnet is present throughout the sample either as semi-rounded aggregates (5–10 mm diameter) separated by sillimanite, biotite and cordierite (Figure 5a); or as highly poikiloblastic, fragmentary (relict) porphyroblasts (1-5 mm). Biotite and sillimanite are commonly included in garnet. Fabric is weakly defined by biotite, sillimanite and quartz, as well as by K-feldspar–rich leucosomes. At hand specimen scale, there is no obvious lineation. The peak mineral assemblage is interpreted to be garnet + sillimanite + cordierite + biotite + quartz + K-feldspar. In places, cordierite is in direct contact with, and partially surrounds garnet (Figure 5b), suggesting that the initial assemblage was garnet + biotite + sillimanite + K-feldspar + ilmenite + magnetite +quartz. In such cases where cordierite and garnet are in contact, inclusions of biotite and sillimanite within the garnet are truncated by cordierite. Coarse-grained cordierite contains abundant and very distinctive pleochroic radiation halos from inclusions of monazite (mostly) and zircon. Cordierite contains inclusions of fine-grained biotite and sillimanite, and remnants of garnet.

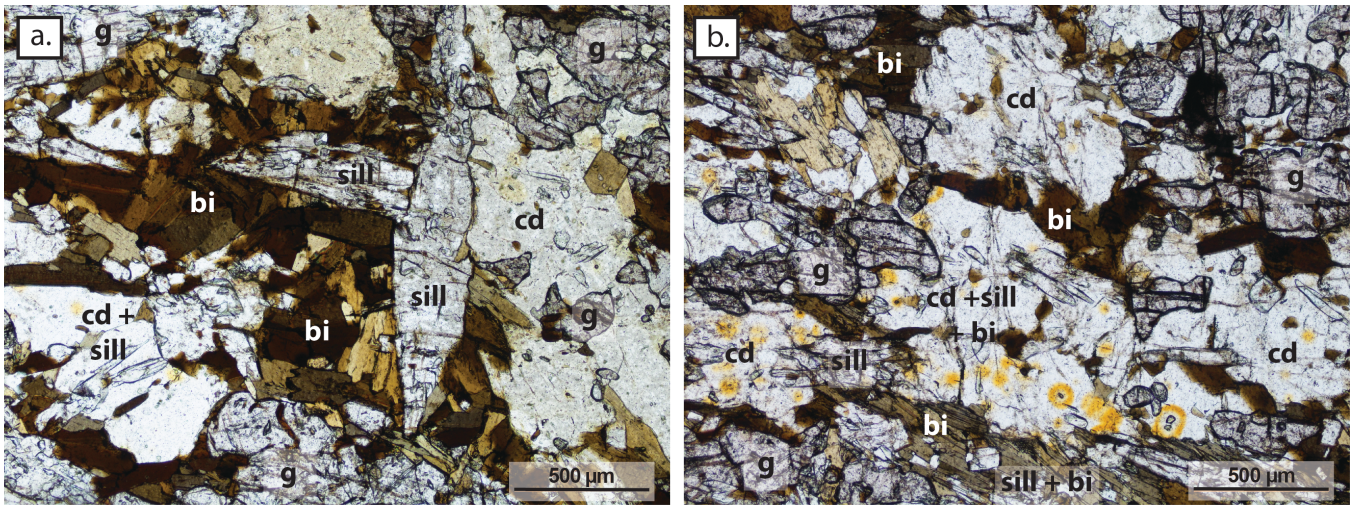

Figure 5: Photomicrographs of key petrological relationships: (a) cordierite partially surrounding garnet, with inclusions of biotite and sillimanite. Coarse grained sillimanite and biotite are also observed. (b) coarse-grained cordierite containing abundant and very distinctive pleochroic radiation halos from the inclusion of monazite; cordierite also contains garnet, biotite and sillimanite inclusions. Garnet is usually observed to be in contact with, or partially surrounded by, cordierite.

6.2 Elemental X-Ray Mapping

Elemental maps for calcium, iron, magnesium and manganese of clustered garnet grains in sample RBN-18 are shown in Figure 6. These elemental maps show that iron gradually increases towards the rim of the garnet (Figure 6a), while magnesium shows a sharp, step-like decrease near the edge of the garnet (Figure 6b). Manganese shows very weak zoning, with a subtle decrease in concentration from core to rim (Figure 6c). However, at the very edge of the garnet grains there is a narrow zone of increased manganese content consistent with resorption of garnet (Spear & Kohn 1996). The calcium distribution (Figure 6d) contrasts with Mn, Mg and Fe, with areas of depletion and enrichment not directly corresponding to zoning from core to rim.

6.3 Pressure-Temperature Conditions

Phase equilibria modelling in the *P-T* domain was undertaken for the metapelitic sample RBN-18 (Figure 7) using the THERIAK-DOMINO software (de Capitani & Petrakakis 2010), for the geologically realistic chemical system SiO_2–Al_2O_3–FeO–Fe_2O_3–MgO–CaO–

Na_2–K_2O–H_2O–TiO_2 (NCKFMASHTO). The interpreted peak mineral assemblage of garnet

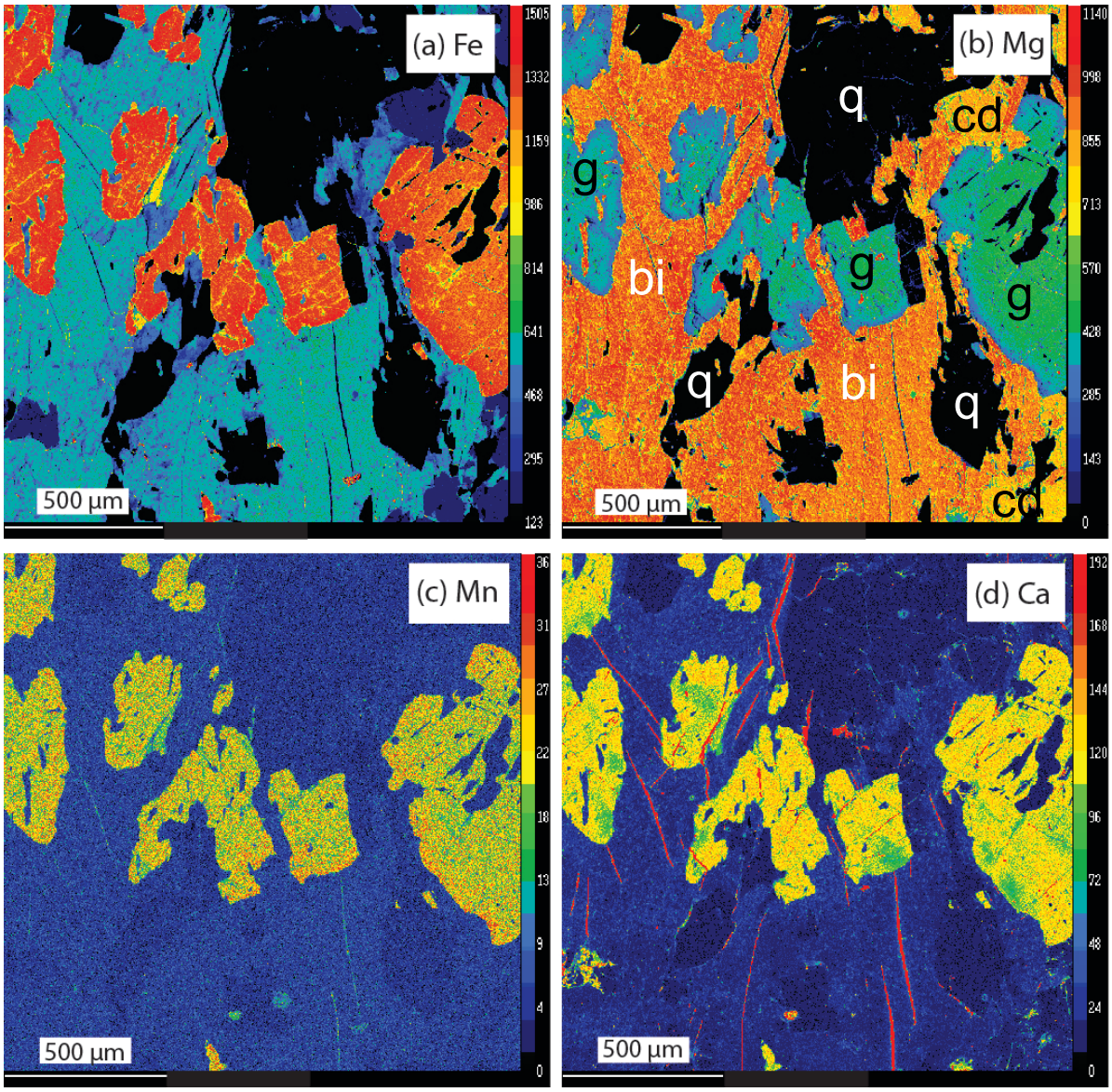

Figure 6: Microprobe elemental maps for iron (Fe), magnesium (Mg), manganese (Mn) and calcium (Ca) for a garnet grain from metapelitic sample RBN-18 assigned to the Illyabba Metamorphics.

sillimanite + biotite + cordierite + K-feldspar + liquid + ilmenite + magnetite + quartz defines *P–T* conditions between approximately 740–900 °C and 7–8 kbar. Cordierite that is in direct contact with, and texturally coronal to, garnet is rich in monazite inclusions and distinct from coarse-grained cordierite elsewhere in the sample that is not rich with monazite inclusions. The monazite-rich cordierite (Figure 5) is interpreted to post-date garnet and could indicate a

decompressive or decompressive-cooling retrograde trajectory (Spear 1994, Figure 7). The black arrow highlights the interpreted *P-T* path based on the change in Mn garnet composition from elemental X-ray mapping and observed reaction textures.

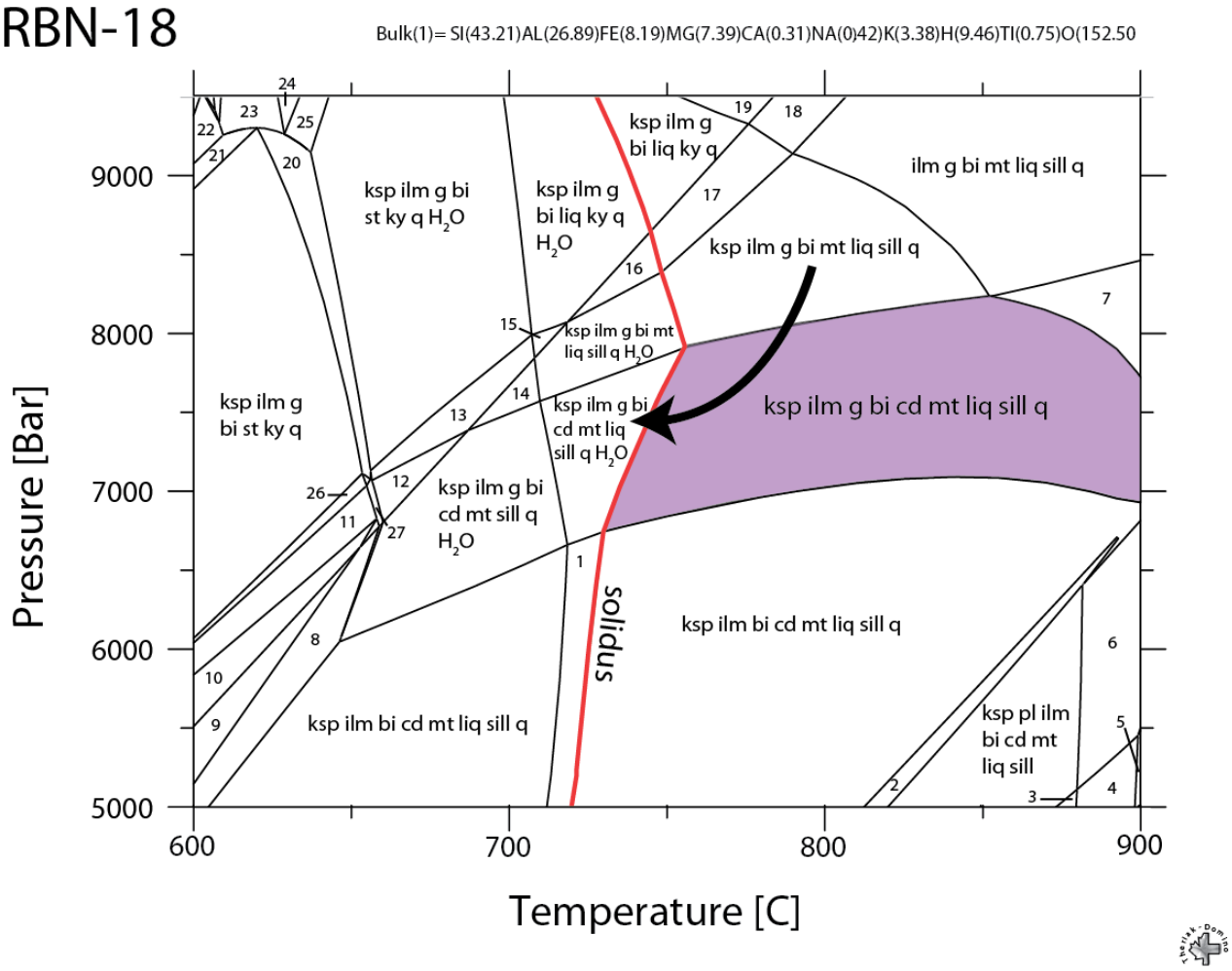

1	ksp ilm bi cd mt liq sill q H_2O	10	ksp ilm bi st cd mt ky sill q	19	ilm g bi liq ky q
2	ksp pl ilm bi cd mt liq sill q	11	ksp ilm g bi st cd mt ky q	20	ksp ilm g bi st ky q H_2O
3	ksp pl ilm cd mt liq sill	12	ksp ilm g bi cd mt ky q H_2O	21	ksp ilm g ph bi st ky q
4	ksp pl ilm cd mt liq sill	13	ksp ilm g bi mt ky q H_2O	22	ilm g ph bi st ky ma q
5	pl ilm cd mt liq sill	14	ksp ilm g bi mt sill q H_2O	23	ilm g ph bi st ky q H_2O
6	pl ilm bi cd mt liq sill	15	ksp ilm g bi mt liq ky q H_2O	24	ilm g ph bi ky q H_2O
7	ilm g bi cd mt liq sill q	16	ksp ilm g bi liq sill q H_2O	25	ksp ilm g ph bi ky q H_2O
8	ksp ilm bi st cd mt sill q H_2O	17	ksp ilm g bi liq sill q	26	ksp ilm g bi st cd ky q
9	ksp ilm bi st cd mt sill q	18	ilm g bi liq sill q	27	ksp ilm g bi st cd mt ky q H_2O

Figure 7: Calculated *P-T* pseudosection for sample RBN-18. The bulk composition is shown above. The numbered list of assemblages corresponds to the numbered fields in the diagram. The solidus is indicated by the solid red line, and the peak field assemblage is highlighted in purple. The black arrow represents the interpreted *P-T* path based on the change in Mn garnet composition from elemental X-ray mapping and observed reaction textures.

6.4 Geochronology

A summary of results for monazite and zircon geochronology are provided in Table 3. Data considered for the calculation of ages in each sample were within ±5% of concordancy. Detailed morphological descriptions of all monazite and zircon samples are provided in Appendix C.

6.4.1 U-Pb MONAZITE LA–ICP–MS GEOCHRONOLOGY

U-Pb monazite data and images of representative grains are shown in Figures 8-10.

Sample RBN-18: metapelite, Illyabba Metamorphics

Thirty analyses were obtained from 28 individual monazite grains. All analyses show less than 5% discordance. A single population is present with a weighted average age of 1616 ± 8 Ma (*n*=30, MSWD=0.24, Figure 8a).

Sample RBN-44: granitic gneiss, Madderns Yard Metamorphic Complex

Twenty analyses were obtained from 16 individual monazite grains. Of the 20 analyses, 2 were rejected outright on the basis of high levels of ^{204}Pb and an additional 2 analyses were excluded (>5% discordance). Sample RBN-44 has a weighted average age of 1071 ± 15 Ma (*n*=16, MSWD=0.59, Figure 8b).

Sample RBN-54: bi–gneiss, Madderns Yard Metamorphic Complex

Thirty-six analyses were obtained from 36 individual monazite grains. The weighted average age of all analyses is 1096 ± 10 Ma (*n*=36, MSWD=0.63, Figure 8c).

Table 3: Summary of U-Pb monazite and zircon geochronology, listed in order of increasing age. The interpretation of age data provided, with data organised in numerous columns to highlight the three main tectonothermal events recorded by the age geochronology data set (un-named Grenvillian event, approximate Liebig event, Inkamulla-Yambah event(s).

	PROVINCE	METAMORPHISM	MAGMATISM	METAMORPHISM	MAGMATISM
U-Pb MONAZITE					
RBN-43	Warumpi	1074 ± 14 Ma (*n*=11)			
RBN-44	Warumpi	1071 ± 15 Ma (*n*=16)			
RBN-54	Warumpi	1096 ± 10 Ma (*n*=36)			
RBN-67	Warumpi/Aileron	1124 ± 10 Ma (*n*=34)			
RBN-71	Aileron	1125 ± 10 Ma (*n*=34)			
RBN-68	Aileron	*c.* 1175 Ma (*n*=4)		*c*. 1615 Ma (*n*=4)	
RBN-18	Aileron			1616 ± 8 Ma (*n*=30)	
RBN-61	Aileron			1625 ± 7 Ma (*n*=33)	
U-Pb ZIRCON					
AS2012-1	Aileron	*c.* 1115 ± 25 Ma^	1633 ± 9 Ma (*n*=33)		
AS2012-2	Aileron	1152 ± 34 Ma (*n*=3)	1629 ± 7 Ma (*n*=44)		
RBN-68	Aileron	1164 ± 19 Ma (*n*=15)	1663 ± 22 Ma^*	*c.* 1654 ± 21 Ma^	*c*. 1770 Ma (*n*=11)
RBN-71	Aileron	*c*. 1142 ± Ma^		*c.* 1610 ± 23 Ma^	*c*. 1780 Ma (*n*=13)
		c. 1222 ± 36 Ma^		*c.* 1678 ± 22 Ma^	
RBN-57	Aileron	*c*. 1111 ± 25 Ma^	*c*. 1612 ± 29 Ma^*		1747 ± 6 Ma (*n*=56)
			c. 1651 ± 23 Ma^*		
RBN-20	Aileron		1626 ± 7 Ma (*n*=43)		
RBN-61	Aileron		*c*. 1629 ± 25 Ma^*		1741 ± 8 Ma (*n*=34)
			c. 1660 ± 24 Ma^*		
RBN-67	Warumpi/Aileron		*c*. 1632 ± 37 Ma^*		*c.* 1760 Ma (*n*=36)
			c. 1643 ± 39 Ma^*		
RBN-54	Warumpi				1764 ± 10 Ma (*n*=19)
RBN-44	Warumpi				1770 ± 7 Ma (*n*=43)
		MODERN DETRITUS POPULATION AGE PEAKS			
HCSS		*c*. 1135 Ma	*c.* 1640 Ma		*c.* 1760 Ma
					MAXIMUM DEPOSITIONAL AGE
RBN-18	Aileron				*c*. 1770 Ma

^ single analysis; * indicates age may be a product of recrystallization.

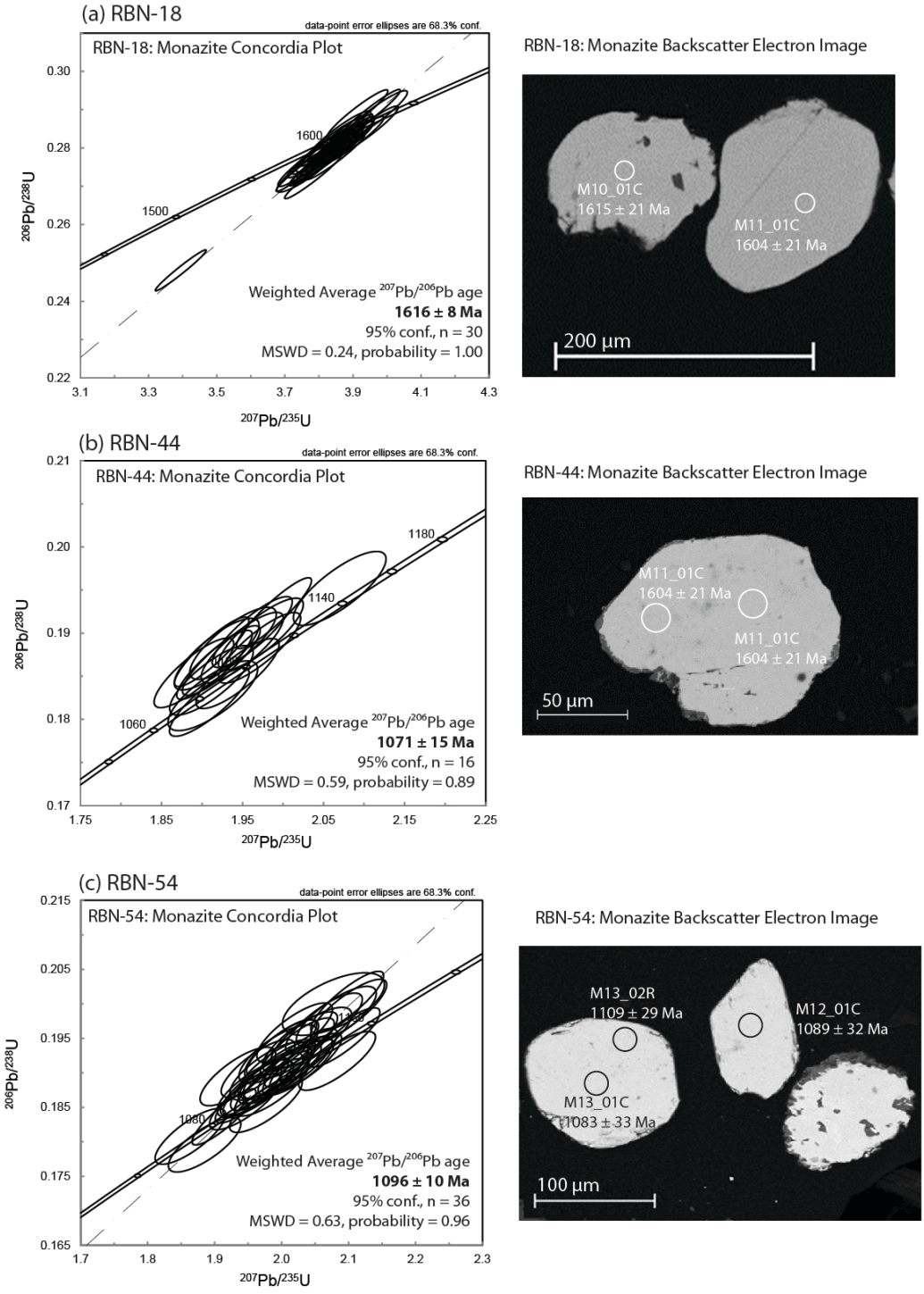

Figure 8: Concordia plots and representative BSE images showing the results of U-Pb monazite geochronology for samples RBN-18, RBN-44 and RBN-54 in this study. All the analyses were conducted on grain mounts of monazite separated from crushed rock using a 15 µm beam width as shown on the BSE images by the black circle. (a) sample RBN-18: One distinct population present, with a weighted average age of 1616 ± 8 Ma (n=30). Grains ranged from euhedral to subhedral in shape and ranged in diameter between ~80–220 µm. Some grains were fractured and some contained inclusions. (b) sample RBN-44: One distinct population present, with a weighted average age of 1071 ± 15 Ma (n=16). Analysed grains were typically subhedral, ranging from rounded to elongate, some grains slightly fractured and containing inclusions; Grains ranged in diameter between ~60–150 µm. (c) sample RBN-54: one distinct age grouping present with a weighted average $^{207}Pb/^{206}Pb$ age of 1096 ± 6 Ma (n=36). Grains analysed could be split into two typical morphologies; the first consisted of euhedral to subhedral and possessed spherical shapes, diameters ranging between ~80–100 µm and did not exhibit zoning in BSE imaging. The second morphological variety was anhedral to subhedral, highly fractured, ~100–200 µm in diameter and contained inclusions.

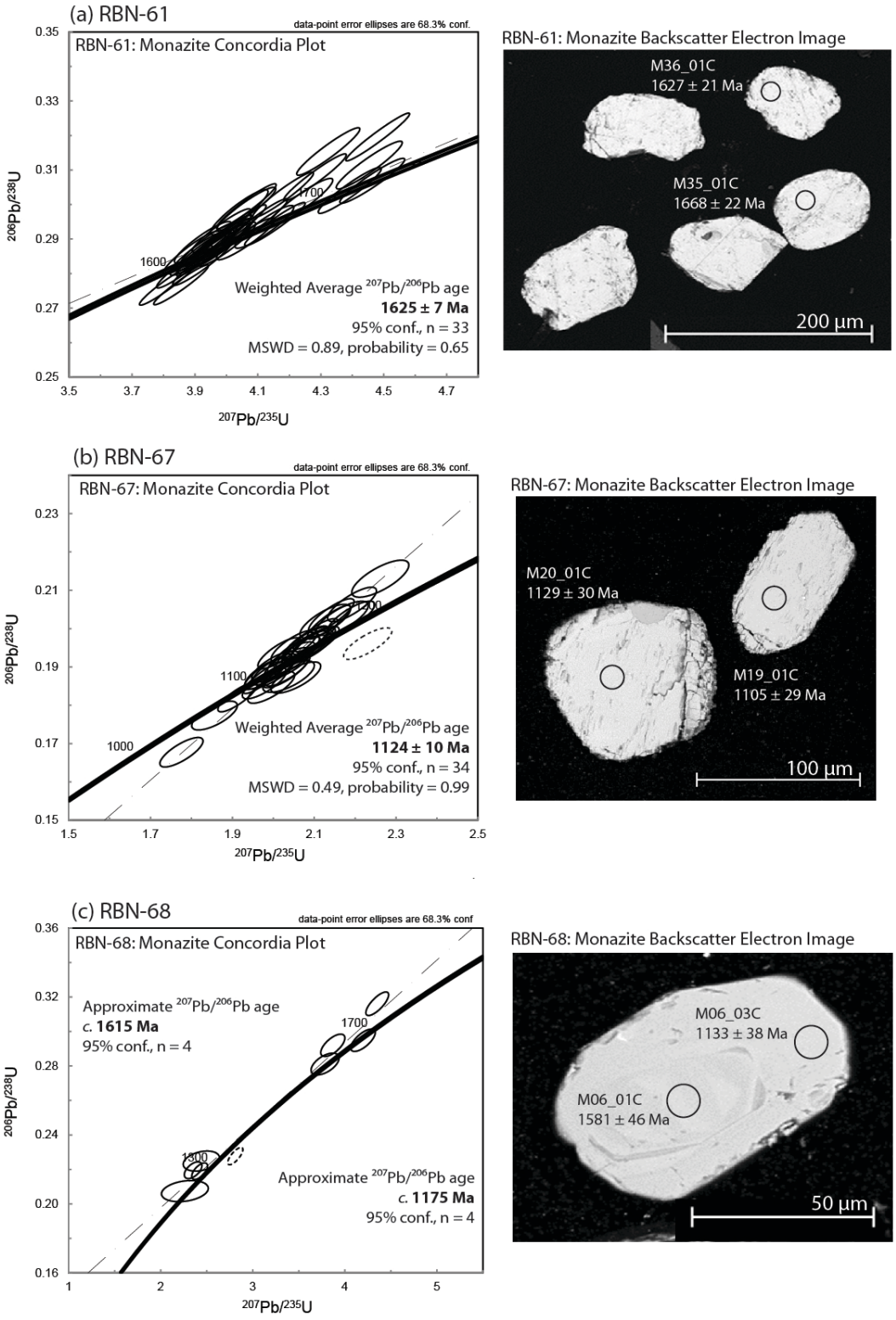

Figure 9: Concordia plots and representative BSE images showing the results of U-Pb monazite geochronology for samples RBN-61, RBN-67 and RBN-68 in this study. All the analyses were conducted on grain mounts of monazite separated from crushed rock using a 15 µm beam width as shown on the BSE images by the black circle. (a) sample RBN-61: One distinct population present, with a weighted average age of 1625 ± 7 Ma (n=33). Analysed grains ranged in diameter between ~80–150 µm, did not appear to be zoned in BSE imaging and were typically euhedral to subhedral and possessed spherical shapes. (b) sample RBN-67: One distinct population present, with a weighted average age of 1124 ± 10 Ma (n=34) and one outlier at 1260 ± 29 Ma. Grains analysed ranged in diameter between ~80–150 µm, did not appear to be zoned in BSE imaging and were typically subhedral, spherical to elongated. (c) sample RBN-68: two age groupings are inferred, with approximate $^{207}Pb/^{206}Pb$ ages of *c.* 1175 Ma (*n*=4) and *c.*1615 Ma (*n*=4) and one outlier at 1416 ± 31 Ma. Concordant grains analysed were typically stubby to spherical and ranged in diameter between ~40–110 µm. Few appeared to be zoned in BSE imaging.

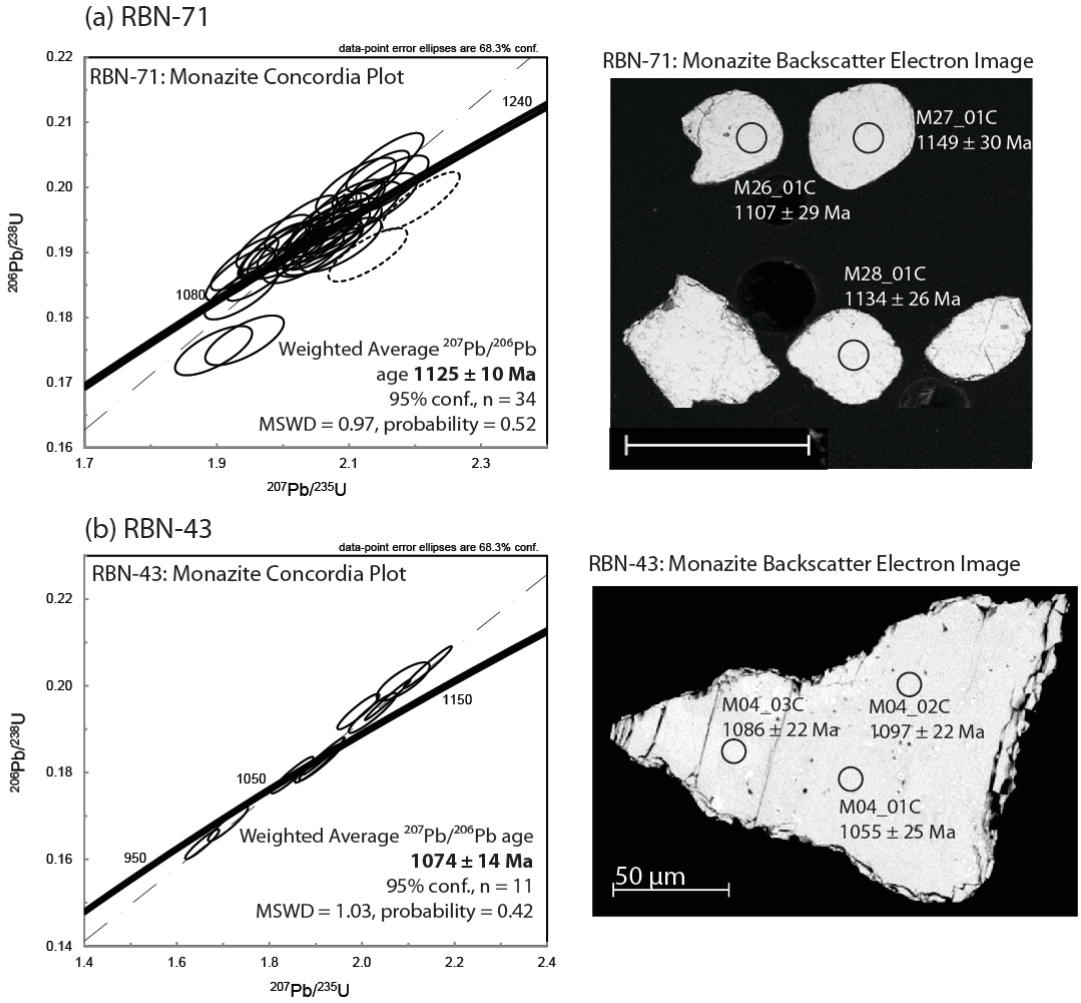

Figure 10: Concordia plots and representative BSE images showing the results of U-Pb monazite geochronology for samples RBN-71 & RBN-43 in this study. All the analyses were conducted on grain mounts of monazite separated from crushed rock using a 15 µm beam width as shown on the BSE images by the black circle. (a) sample RBN-71: One distinct population present, with a weighted average $^{207}Pb/^{206}Pb$ age of 1125 ± 10 Ma (n=34) and two outliers (1221 ± 27 Ma & 1232 ± 31 Ma). Analysed grains ranged in diameter between approximately 80–250 µm, did not appear to be zoned in BSE imaging, and were typically euhedral to subhedral with spherical shapes. (b) sample RBN-43: One distinct population present, with a weighted average $^{207}Pb/^{206}Pb$ age of 1074 ± 14 Ma (n=11). Grains analysed ranged in diameter between ~80–150 µm, did not appear to be zoned in BSE imaging and were typically subhedral, spherical to elongated.

Sample RBN-61: migmatitic orthogneiss, Illyabba Metamorphics

Thirty-six analyses were obtained from 36 individual monazite grains. From all analyses, a single age population is present with a weighted average age of 1625 ± 7 Ma (*n*=33, MSWD=0.89, Figure 9a).

Sample RBN-67: quartzofeldspathic gneiss, Old Hamilton Downs Gneiss

Thirty-seven analyses were obtained from 23 individual monazite grains. Of the 37 analyses, 2 were excluded (>5% discordance). One additional outlying analysis was excluded (1260 ± 29 Ma). Sample RBN-67 has a weighted average age of 1124 ± 10 Ma (*n*=34, MSWD=0.49, Figure 9b).

Sample RBN-68: granitic gneiss, Illyabba Metamorphics

Twenty-two analyses were obtained from 11 individual grains. Of the 22 analyses, 1 was rejected outright due to noisy time-resolved signals, and a further 7 analyses were excluded (>5% discordance). Given the scarcity of concordant data, conservatively two main populations can be inferred; the ages of these populations are *c*. 1175 Ma (*n*=4) and *c.* 1615 Ma (*n*=4, Figure 9c). One outlying analysis was excluded from age calculations (1416 ± 31 Ma).

Sample RBN-71: granitic gneiss, Old Hamilton Downs Gneiss

Thirty-seven analyses were obtained from 36 individual monazite grains. Of the 37 analyses, 1 was rejected outright (>10% discordance). Sample RBN-71 has a weighted average age of 1125 ± 10 Ma (*n*=34, MSWD=0.97, Figure 10a). Two outlying analyses were excluded (1221 ± 27 Ma & 1232 ± 31 Ma).

Sample RBN-43: pegmatite with seam of euhedral garnet, Madderns Yard Metamorphic Complex

Twenty-one analyses were conducted on ten individual monazite grains. Of the 21 analyses, 3 were rejected outright due to noisy time-resolved signals, and a further 7 analyses were excluded (>5% discordance). Sample RBN-43 has a weighted average age of 1074 ± 14 Ma (*n*=11 MSWD=1.03, Figure 10b).

6.4.2 U-Pb ZIRCON LA-ICP-MS GEOCHRONOLOGY

U-Pb zircon data and images of representative grains are shown in Figures 11-14 (zircon); Figure 14 also displays detrital age spectra for relevant samples. Th/U plots for relevant samples are given in Figure 15.

Sample AS2012-1: migmatitic granitic gneiss, Illyabba Metamorphics

Sixty-six analyses were obtained from 31 individual grains. Of the 66 analyses, 17 were excluded (>5% discordance). The main population for AS2012-1 has a weighted average age of 1633 ± 9 Ma (*n*=33, MSWD=0.35, Figure 11a); the sample contained 2 older outliers, at 1719 ± 32 Ma and 1729 ± 21 Ma. A single younger outlier gave an age of 1115 ± 25 Ma (97% conc., Th/U = 0.03). A plot of Th/U ratio vs age for AS2012-1 is shown in Figure 15a. The zircon analyses are characterised by a large range in Th/U values, with many clustering between ~0.2-0.97 (*n*=35).

Sample AS2012-2: migmatitic orthogneiss, Illyabba Metamorphics

Seventy-eight analyses were obtained from 52 individual grains. Of the 78 analyses, 30 were excluded (>5% discordance). Two distinct age clusters are present in AS2012-2: a smaller (*n*=3), younger 'population' collected from weakly to highly luminescent rims of zircons (Figure 11b) and a larger (*n*=44), older population collected from zircon cores and areas of oscillatory zoning (Figure 11b). The sample contained 1 older outlier (1724 ± 25 Ma). AS2012-2 has an older population with a weighted average age of 1629 ± 7 Ma (*n*=44, MSWD=0.59). The younger age 'population' gave a weighted average age of 1152 ± 34 Ma (*n*=3, MSWD=0.49, Figure 11b). A plot of Th/U ratio vs age for AS2012-2 is shown in Figure 15b. The zircon analyses are characterised by a large range in Th/U values with a large cluster between ~0.1-0.8 (*n*=43). Three analyses are characterised by very low Th/U

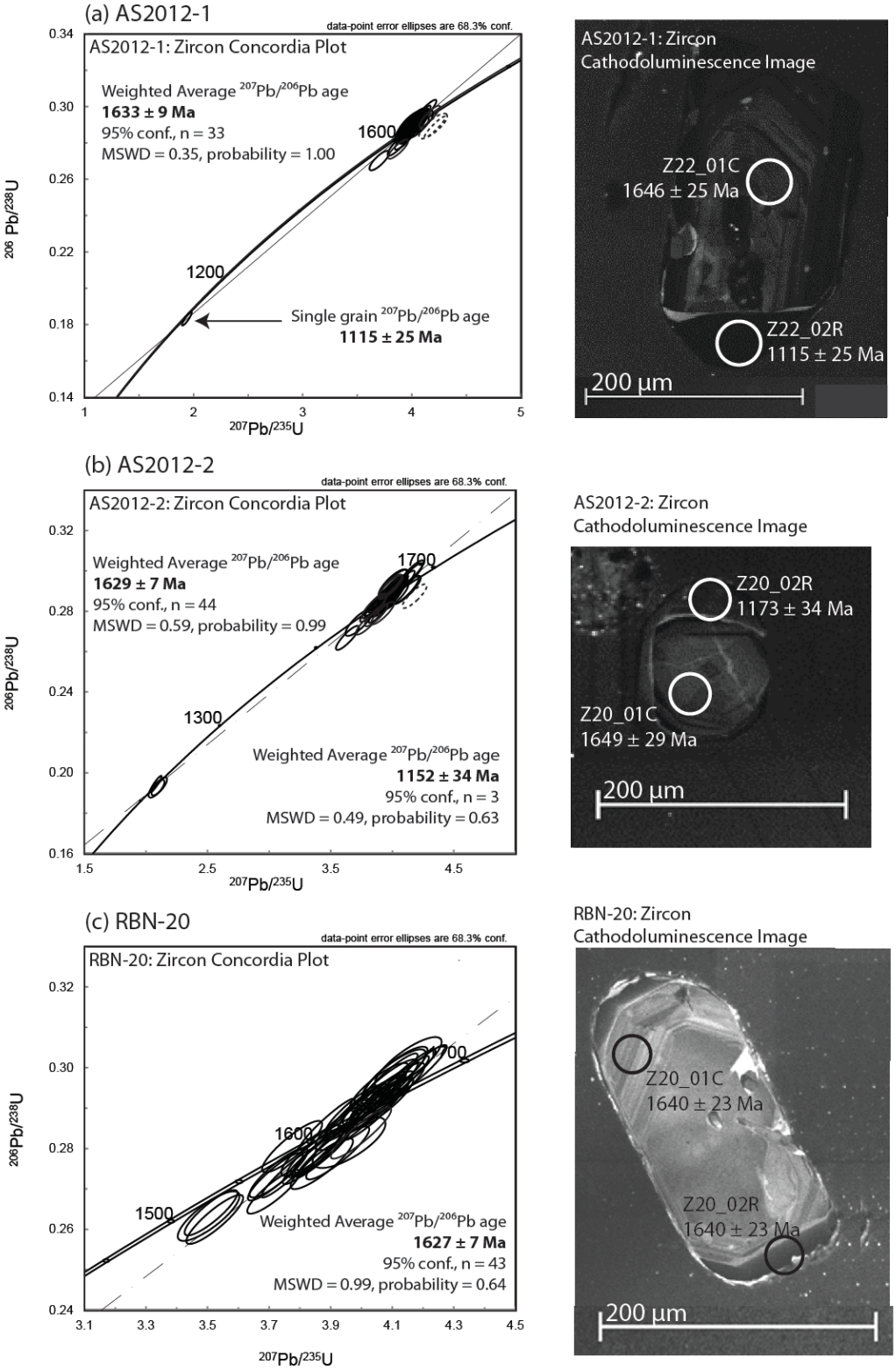

Figure 11: Concordia plots and representative cathodoluminescence (CL) images showing the results of U-Pb zircon geochronology for samples RBN-20, AS2012-1 & AS2012-2 analysed in this study. All the analyses were conducted on grain mounts of zircons separated from crushed rock, using a 30 µm beam width as shown on the CL images with a black circle. (a) AS2012-1: two age groupings are inferred; one older age population with a weighted average $^{207}Pb/^{206}Pb$ age of 1633 ± 9 Ma (*n*=33), a younger, single grain analysis (1115 ± 25 Ma) and two outliers (1719 ± 32 Ma & 1729 ± 21 Ma). Grains typically elongate, euhedral–subhedral and rounded edges. ~120–400 µm diameter, aspect ratios of 1:3. Most are fractured, with weak to highly luminescent oscillatory zoning with a mixture of strongly to weakly luminescent rims. (b) AS2012-2: two distinct age populations with weighted average $^{207}Pb/^{206}Pb$ ages of 1152 ± 34 Ma (*n*=3) and 1629 ± 7 Ma (*n*=44), and two outliers (1615 ± 28 Ma, 1608 ± 24 Ma). Rounded to elongate, euhedral–subhedral and rounded edges. ~80–400 µm with aspect ratios of 1:3. Most grains are fractured and exhibit weak to highly luminescent oscillatory zoning with a mixture of strongly to weakly luminescent rims. Mostly convoluted cores. (c) RBN-20: One distinct population present, with a weighted average age of 1627 ± 7 Ma (*n*=43). Grains are typically stubby to elongate, euhedral–subhedral and mostly rounded edges. ~80–420 µm. Most grains contain fractures and exhibit weak to highly luminescent oscillatory zoning. Most grains exhibit xenocrystic cores, some convoluted.

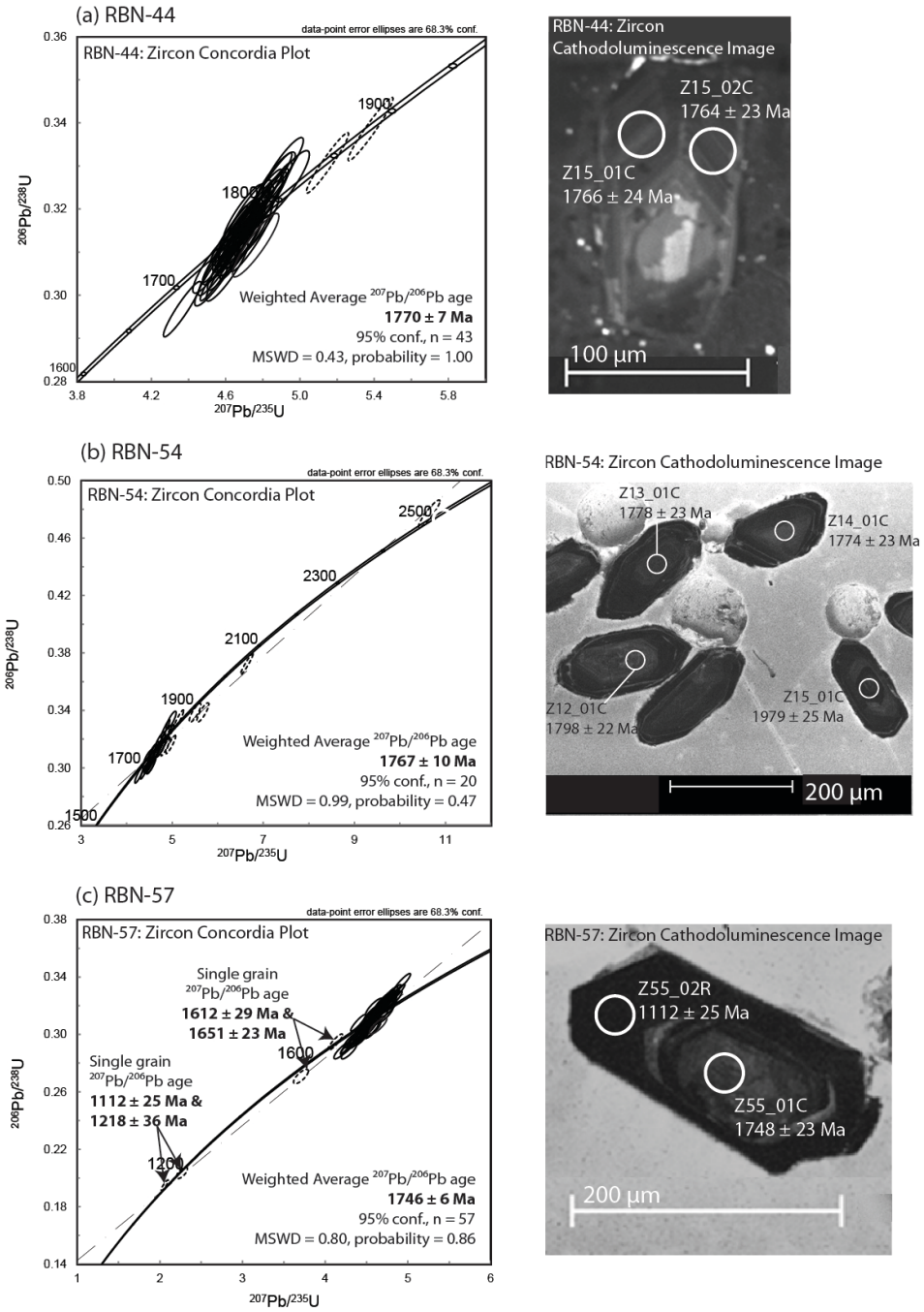

Figure 12: Concordia plots and representative cathodoluminescence (CL) images showing the results of U-Pb zircon geochronology for samples RBN-44, RBN-54 & RBN-57 analysed in this study. All the analyses were conducted on grain mounts of zircons separated from crushed rock, using a 30 µm beam width as shown on the CL images with a black circle. (a) RBN-44: One distinct population present, with a weighted average age of 1770 ± 7 Ma (*n*=43) and two outliers (1846 ± 20 Ma & 1883 ± 20 Ma). Grains are typically equant to stubby, euhedral–subhedral with rounded edges. ~80–200 µm in length. Most grains contain fractures, weak to moderate luminescence, rare oscillatory zoning and some convoluted cores. (b) RBN-54: One distinct population present, with a weighted average age of 1767 ± 10 Ma (*n*=20) A number of analyses from inherited grains were not included in the weighted average. Grains are typically stubby to elongate, euhedral-subhedral and have rounded edges. ~80–200 µm in length. Most grains contain fractures and exhibit weakly luminescent, well-defined concentric oscillatory and sector zoning. Some grains exhibit convoluted and/or xenocrystic cores. (c) RBN-57: One distinct population present, with a weighted average age of 1746 ± 6 Ma (*n*=57) and four younger outliers (*c.* 1110 – *c.* 1650 Ma). Grains are typically stubby to elongate, euhedral–subhedral and mostly rounded edges. ~80–420 µm. Most grains contain fractures and exhibit weak to highly luminescent oscillatory zoning. Most grains exhibit xenocrystic cores, some convoluted. Grains are typically stubby to elongate, euhedral-subhedral and have rounded edges. ~100–250 µm in length. Most grains are fractured and exhibit weakly luminescent, well-defined concentric oscillatory and sector zoning. Some grains exhibit convoluted and/or metamict cores.

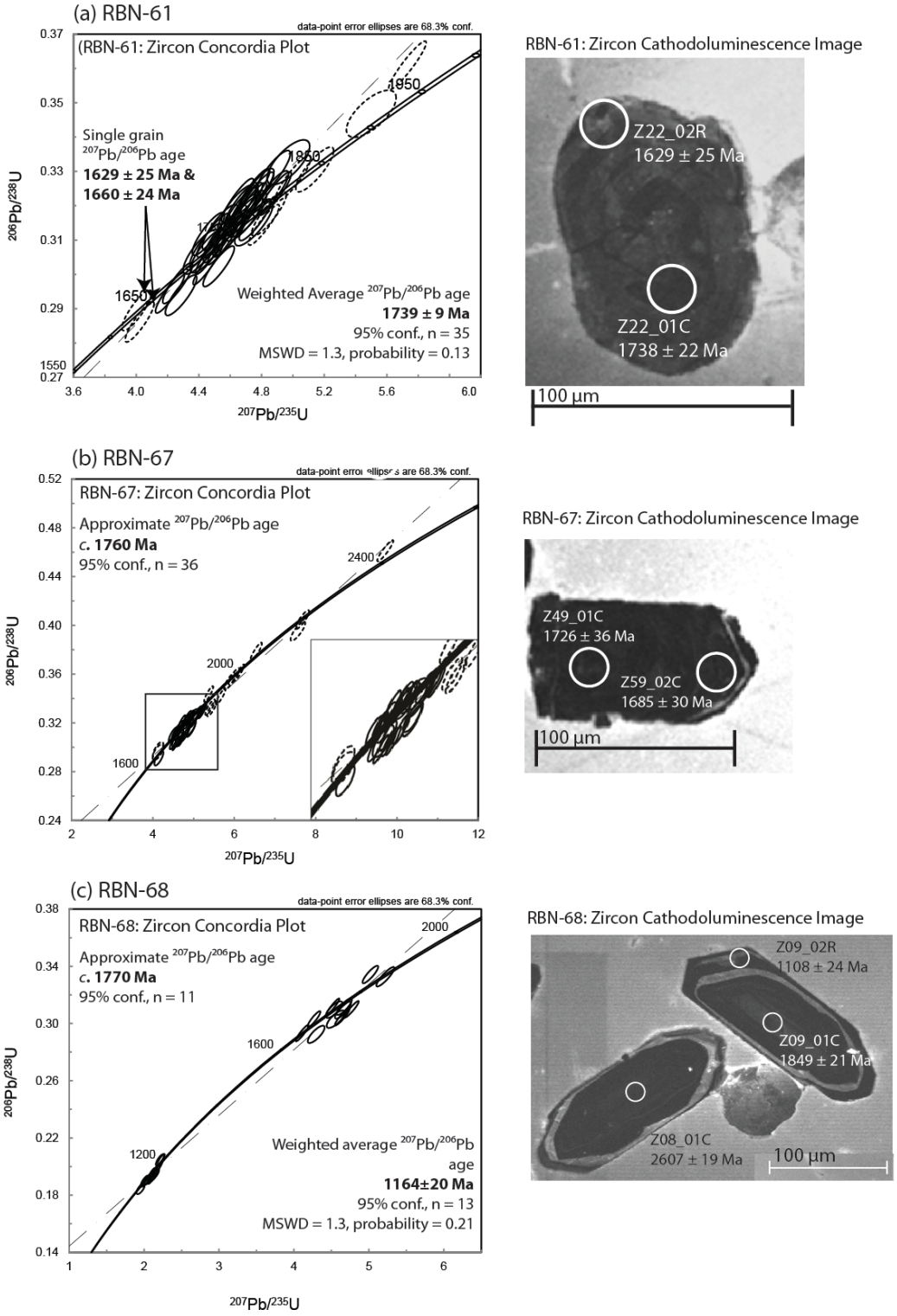

Figure 13: Concordia plots and representative cathodoluminescence (CL) images showing the results of U-Pb zircon geochronology for samples RBN-61, RBN-67 & RBN-68 analysed in this study. All the analyses were conducted on grain mounts of zircons separated from crushed rock, using a 30 µm beam width as shown on the CL images with a black circle. (a) RBN-61: One distinct population present, with a weighted average $^{207}Pb/^{206}Pb$ age of 1739 ± 9 Ma (*n*=35) and two outliers (1629 ± 25 Ma & 1660 ± 24 Ma). A number of analyses from inherited grains were not included in the weighted average. Grains are typically stubby to elongate, euhedral-anhedral and have rounded edges. ~80–400 µm in length. Most grains are highly fractured and exhibit weakly luminescent, poorly-defined concentric oscillatory and sector zoning. Some grains exhibit convoluted and/or metamict cores, and local recrystallization. (b) RBN-67: One age population present, with an approximate $^{207}Pb/^{206}Pb$ age of *c.* 1760 Ma (*n*=11). A large number of analyses from inherited grains are present. Grains are typically stubby to elongate, euhedral-subhedral and have rounded edges. ~100–250 µm in length. Most grains are fractured and exhibit weakly luminescent, poorly-defined concentric oscillatory and sector zoning. (c) sample RBN-68: two distinct age populations with a weighted average $^{207}Pb/^{206}Pb$ age of 1164 ± 20 Ma (*n*=13) and an approximate $^{207}Pb/^{206}Pb$ age of *c.* 1770 Ma (*n*=11). Grains are typically stubby to elongate, euhedral-subhedral and have rounded edges. ~100–250 µm in length. Most grains are fractured and exhibit weakly luminescent, well-defined concentric oscillatory and sector zoning. Some grains exhibit convoluted and/or metamict cores.

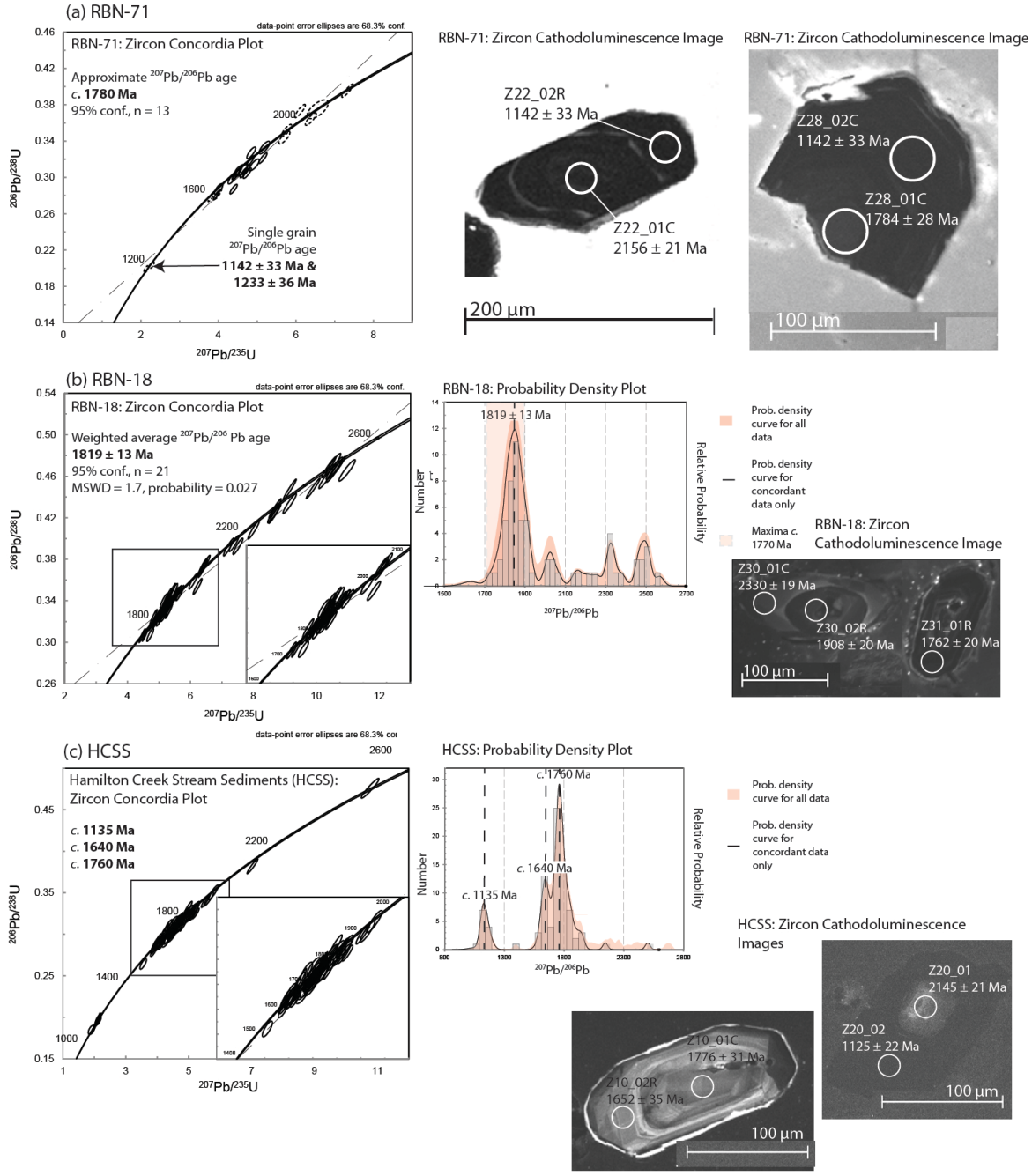

Figure 14: Concordia plots and representative cathodoluminescence (CL) images showing the results of U-Pb zircon geochronology for sample RBN-71, and U-Pb detrital zircon geochronology for samples RBN-18 & HCSS analysed in this study. All the analyses were conducted on grain mounts of zircons separated from crushed rock, using a 30 µm beam width as shown on the CL images with a black circle. (a) RBN-71: One main age grouping present, with an approximate $^{207}Pb/^{206}Pb$ age of *c.* 1780 Ma (*n*=13) and two younger outliers (1142 ± 33 Ma & 1233 ± 36 Ma). A number of analyses from inherited grains were not included in the weighted average. Grains are typically stubby to elongate, euhedral-subhedral and have rounded edges. ~100–250 µm in length. Most grains are fractured and exhibit weakly luminescent, poorly-defined concentric oscillatory and sector zoning. Some grains exhibit convoluted and/or metamict cores, and local recrystallisation (b) RBN-18: Concordia plot and age spectra plot display the range of detrital zircon ages (*n*=60). Grains typically exhibit weakly to highly luminescent oscillatory zoning, and weakly luminescent domain zoning. Some grains exhibited transgressive overgrowths and convoluted cores. A significant proportion of larger grains (~200–250 µm in length) exhibit dark, non-luminescent cores and moderately luminescent rims. (c) sample HCSS: Concordia plot and age spectra plot display the range of detrital zircon ages (*n*=87) Grains are typically stubby to elongate, euhedral-subhedral and have rounded edges. ~100–250 µm in length. Most grains are fractured and exhibit weakly luminescent, well-defined concentric oscillatory and sector zoning. Some grains exhibit convoluted and/or metamict cores. Grains range from euhedral to subhedral, and stubby to elongate. The fraction of smaller grains are ~80–200 µm in length, the larger translucent brown fraction (approximately 30%) are ~200–400µm in length. Grains are fractured, the larger fraction typically exhibits weak luminescent oscillatory and domain zoning, while the smaller fraction of grains typically exhibits moderately to highly luminescent oscillatory and featureless domain zoning. Some grains exhibit transgressive overgrowths and convoluted metamorphic cores, and a large proportion have dark featureless cores with highly luminescent rims.

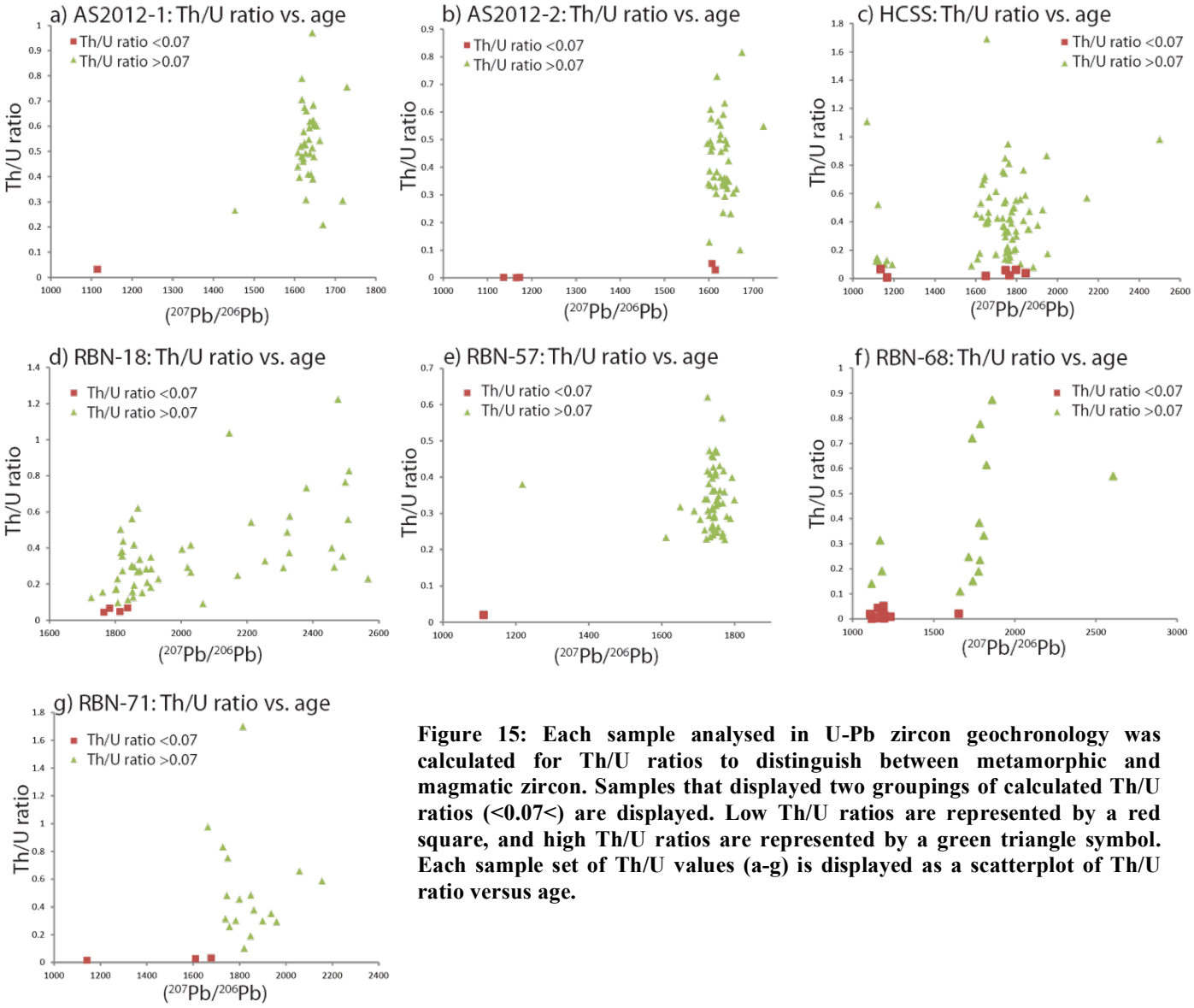

Figure 15: Each sample analysed in U-Pb zircon geochronology was calculated for Th/U ratios to distinguish between metamorphic and magmatic zircon. Samples that displayed two groupings of calculated Th/U ratios (<0.07<) are displayed. Low Th/U ratios are represented by a red square, and high Th/U ratios are represented by a green triangle symbol. Each sample set of Th/U values (a-g) is displayed as a scatterplot of Th/U ratio versus age.

ratio. (<0.002, *c.* 1135–1175 Ma). Another 2 analyses have low Th/U values; 0.03 (1615 ± 28 Ma) and 0.05 (1608 ± 24 Ma).

Sample RBN-20: Folded porphyroclastic granite, Illyabba Metamorphics

Sixty-two analyses were obtained from 34 individual grains. Of the 62 analyses, 19 were excluded (>5% discordance). A single population is present with a weighted average age of 1627 ± 7 Ma (*n*=43, MSWD=0.92, Figure 12c). The zircon analyses are characterised by a moderate range in Th/U values (0.31–0.77, *n*=43).

Sample RBN-44: granitic gneiss, Madderns Yard Metamorphic Complex

Sixty-five analyses were obtained from 57 individual grains. Of the 65 analyses, 18 were excluded (>5% discordance). The main population for RBN-44 has a weighted average age of 1770 ± 7 Ma (*n*=43, MSWD=0.43, Figure 13a). The main cluster of zircon analyses are characterised by a narrow range in Th/U values (0.2–0.44, *c.* 1740–1813 Ma, *n*=43). Two outliers gave ages of 1846 ± 20 Ma (Th/U=0.17) and 1883 ± 20 Ma (Th/U=0.09).

Sample RBN-54: bi–gneiss, Madderns Yard Metamorphic Complex

Forty-five analyses were obtained from 35 individual grains. Of the 45 analyses, 17 were excluded (>5% discordance). The main population for RBN-54 has a weighted average age of 1767 ± 10 Ma (*n*=20, MSWD=0.99, Figure 13b). Eight older, concordant outliers gave ages ranging between *c.* 1809–2476 Ma. The main cluster of zircon analyses is characterised by a moderate range in Th/U values (Th/U = 0.13–0.52, *c.* 1714–2089 Ma, *n*=27). One outlying analysis has an age of 2476 ± 20 Ma (Th/U = 0.63).

Sample RBN-57: Megacrystic ksp–gneiss, Illyabba Metamorphics

Seventy-seven analyses were obtained from 66 individual grains. Of the 77 analyses, 17 were excluded (>5% discordance). The main population for RBN-57 has a weighted average age of 1746 ± 6 Ma (*n*=56, MSWD=0.69, Figure 13c). A plot of Th/U ratio vs age for RBN-57 is shown in Figure 15e. The main cluster of zircon analyses are characterised by a large range in Th/U values (0.23–0.62), with ages of *c.* 1689–1799 Ma (*n*=56). Two younger, concordant outliers gave ages of 1612 ± 29 Ma (96% conc., Th/U = 0.23) and 1651 ± 23 Ma (101% conc., Th/U = 0.32). Another 2 outlying analyses gave ages of 1112 ± 25 Ma (103% conc., Th/U = 0.02) and 1218 ± 36 (98% conc., Th/U = 0.38).

Sample RBN-61: migmatitic orthogneiss, Illyabba Metamorphics

Fifty-nine analyses were obtained from 35 individual grains. Of the 59 analyses, 16 were excluded (>5% discordance). The main population for RBN-61 has a weighted average age of 1739 ± 9 Ma (*n*=35, MSWD=1.3, Figure 13a). Six older, outlying analyses range between *c.* 1810–1884 Ma. The main cluster of zircon analyses are characterised by a large range in Th/U values (0.078–0.67) with ages of *c.* 1692–1884 Ma (*n*=27). Two younger, concordant outliers gave ages of 1629 ± 25 Ma (101% conc., Th/U = 0.19) & 1660 ± 24 Ma (98% conc., Th/U = 0.17). Fourteen analyses gave low Th/U values (0.01–0.07) between the ages of *c.* 1711–1818 Ma.

Sample RBN-67: quartzofeldspathic gneiss, Old Hamilton Downs Gneiss

Sixty-eight analyses were obtained from 61 individual grains. Of the 68 analyses, 25 were excluded (>5% discordance). The main population for RBN-67 has an approximate age of *c.* 1760 Ma (*n*=36, Figure 13b). The main distribution of zircon analyses have Th/U values of ~0.14–0.66 with ages of *c.* 1685–2033 Ma (*n*=36). There are three older, concordant outliers with ages ranging *c*. 2196–2376 Ma (97-103% conc., Th/U = 0.33–1.2). Two younger, concordant outliers gave ages of 1632 ± 37 Ma (103% conc., Th/U = 0.47) & 1643 ± 39 Ma (102% conc., Th/U = 0.66).

Sample RBN-68: granitic gneiss, Illyabba Metamorphics

Sixty-five analyses were obtained from 56 individual grains. Of the 65 analyses, 39 were excluded (>5% discordance). Two distinct populations are present in RBN-68. The older population has an approximate age of *c.* 1770 Ma (*n*=11) with concordancy ranging between 95–104%. The younger population gave a weighted average age of 1164 ± 19 Ma (*n*=13, MSWD=1.3, Figure 13c). A plot of Th/U ratio vs age for RBN-68 is shown in Figure 15f. The plot shows there are two main clusters of zircon analyses. The younger cluster (*c.* 1108–1234 Ma) is characterised by a large range in Th/U values (0.0009–0.31, *n*=10). The older

cluster is also characterised by a large, but generally higher range of Th/U values (0.11–0.87, *n*=14). There are two outlying analyses with ages of 1654 ± 21 Ma (100% conc., Th/U = 0.02) & 2607 ± 19 Ma (100% conc., Th/U = 0.57).

Sample RBN-71: granitic gneiss, Old Hamilton Downs Gneiss

Fifty-five analyses were obtained from 61 individual grains. Of the 55 analyses, 32 were rejected outright on the basis of excessive discordance (>10%) and high levels of ^{204}Pb. An additional 2 were excluded (>5% discordance). The main age population for RBN-71 has an approximate age of *c.* 1780 Ma (*n*=13, Figure 14a). Six older, outlying analyses range between *c.* 1937–2385 Ma (95–100% conc.). A plot of Th/U ratio vs age for RBN-71 is shown in Figure 15g. The main cluster of zircon analyses are characterised by a large range in Th/U values (0.1–1.7) with ages of *c.* 1664–2156 Ma (*n*=18). Three younger, concordant outliers gave ages of 1142 ± 33 Ma (102 conc., Th/U = 0.02), 1610 ± 23 Ma (98% conc., Th/U = 0.03) and 1678 ± 22 (95% conc., Th/U = 0.03).

6.4.3 U-Pb DETRITAL ZIRCON LA-ICP-MS GEOCHRONOLOGY

Sample RBN-18: metapelite, Illyabba Metamorphics

Sixty-four analyses were conducted on 67 individual zircon grains, targeting grain cores and regions of oscillatory zoning. Of the 64 analyses, 4 were excluded (>5% discordance). The weighted average age of the youngest (and most populated) peak is 1819 ± 13 Ma (*n*=21, MSWD=1.7) and is yielded from both rims and cores of grains, typically oscillatory zoned and moderate to weakly luminescent zoned grains. The youngest concordant grains gave ages of 1727 ± 21 Ma (100% conc.) and 1762 ± 20 Ma (98% conc.). The 1727 Ma single grain analysis is an outlier from the main population. There is a broad range of age data between *c.* 1850 and *c.* 2570 Ma, with minor peaks at *c.* 2030 Ma, *c.* 2160 Ma, *c.* 2330 Ma and *c.* 2500 Ma (Figure 14b) typically emerging from weakly luminescent oscillatory zoned, weak to

moderately luminescent oscillatory zoned, and highly luminescent domain zoned grains respectively. A plot of Th/U ratio vs. age for RBN-18 is shown in Figure 15d. The zircon analyses are characterised by a large range in Th/U values (0.04–1.2) across the detrital age spectra.

6.4.4 U-Pb MODERN STREAM SEDIMENT ZIRCON LA-ICP-MS GEOCHRONOLOGY

Hamilton Creek Stream Sediment (HCSS)

One hundred and thirty nine (139) analyses were obtained from 111 individual zircon grains from sample HCSS (figure 14c). Of the 139 analyses, 7 were rejected outright on the basis of noisy isotopic ratios and high levels of ^{204}Pb. An additional 45 analyses were excluded (>5% discordance). Figure 14c shows three significant peaks in the detrital zircon age spectra at *c.* 1135 Ma, *c.* 1640 Ma and *c.* 1760 Ma. The age spectrum ranges from the youngest concordant grain at 1068 ± 69 Ma, up to the oldest concordant grain at 2500 ± 21 Ma. A plot of Th/U ratio vs age for HCSS is shown in Figure 15c. The zircon analyses are separated into two clusters; the smaller, younger cluster (*c.* 1135 Ma) is characterised by a large range in Th/U values (0.007–1.6, *n*=12); the older, larger cluster (*c*. 1760 Ma) is also characterised by a large range in Th/U values (0.02–1.7, *n*=68). One single outlier gave an age of 2500 ± 21 Ma (100% conc., Th/U = 0.98).

7 DISCUSSION

The geochronological data collected in this study has been targeted at structurally constrained samples, in an attempt to define the age of fabric elements and different structural domains. As such, the geochronological data set provides significant constraints in understanding the geological history of the Arunta region and underpinning tectonic models that may be derived from such essential data.

7.1 Interpretation of Geochronology

7.1.1 MONAZITE U-Pb AGE DATA

It is generally recognised that in high grade metamorphic rocks monazite forms part of the metamorphic assemblage and therefore can provide constraints on the timing of metamorphism (and associated deformation; Kingsbury *et al*. 1993, Kelly *et al.*2006). In the monazite U-Pb age data collected in this study there are clearly two age populations (Table 3). The older age population ranges between *c.* 1625 and 1615 Ma and the younger ages range between *c.* 1175 and 1070 Ma. The *c.* 1625–1615 Ma ages are documented from metapelitic sample RBN-18, megacrystic (and migmatitic) orthogneiss RBN-61 and, less confidently, from a biotite-poor granitic gneiss (RBN-68). The 1616 ± 8 Ma age recorded by metapelitic sample RBN-18 is likely to reflect metamorphism at this time, as no record of older events is preserved by monazite, and the zircon in this sample (see section 7.1.2) is considered to be detrital only. Although the textural location of the analysed monazite is unknown, the proportion of grains within late stage cordierite (Figure 5) in the sample makes it likely that the bulk of the analysed grains come from within late-stage mineral growths in the sample. If this is the case, then 1616± 8 Ma age may correspond to the inferred decompression/cooling setting.

Many of the samples record ages corresponding to the Grenvillian-aged Teapot Thermal Event (Morrissey *et al.* 2011; Wong 2011) and also the Musgrave Orogeny (Smithies *et al.* 2011). These samples (RBN-43, -54, -44, -67, -71 and -68; see Table 3) come from both the Warumpi and Aileron Provinces, based on the definition that the Charles River Thrust is the boundary between the two provinces in the study area (Northern Territory Geological Survey 2012). As these samples either contain older ages, are pegmatitic (in the case of RBN-43), or situated proximal to E-W trending mylonites or high-strain zones, the Grenvillian-aged monazite data is interpreted to reflect reworking and partial melting during this period. This

is consistent with recent work by Morrissey *et al*. (2011) and Wong (2011) that documented widespread and near-pervasive Grenvillian-aged reworking of the southern Arunta Region.

Sample RBN-68, in contrast to the previously discussed samples with single age populations, displays a range of monazite $^{207}Pb/^{206}Pb$ ages from *c*. 1140 – *c*. 1680 Ma (Figure 9c). The closure temperature of monazite has been shown to be a function of grain size, cooling rate and other influences such as fluids and recrystallization (Kelsey *et al.* 2003, Kelly *et al.* 2006, Kelsey *et al.* 2008). Therefore, sufficiently large monazite grains (~ >50-100 μm) can have U-Pb growth ages remain unaffected by temperatures in excess of 750-800°C in later metamorphic events (Rubatto *et al.* 2001). RBN-68 contains monazite ranging in size between approximately 50-100 μm, therefore making it plausible for the preservation of more than one monazite population within the same sample.

7.1.2 ZIRCON U-Pb AGE DATA

U-Pb zircon data from rock samples correlates well with the age spectra from the stream sediment sample HCSS. The age ranges/peaks are present: *c.* 1780 and 1740 Ma, *c.* 1680 to 1610 Ma and *c.* 1160 and 1110 Ma (Figure 14c).

The oldest population, delineated at *c.* 1760 Ma in sample HCSS, is derived predominantly from cores of zircon grains (usually exhibiting oscillatory zoning, Figure 14c) and is therefore interpreted as magmatic. Samples that contain the *c.* 1760 Ma ages occur to the north and south of the Charles River Thrust, and therefore occur in the Aileron as well as Warumpi Provinces.

The middle population, delineated at *c.* 1640 Ma in sample HCSS, is derived from oscillatory and sector zoned, moderate to highly luminescent zircon cores (some convoluted) and occasional metamorphic rims, recognised as overgrowths (Figure 14c, Corfu *et al.* 2003); this

age is interpreted as magmatic for samples AS2012-1, AS2012-2 and RBN-20 on the basis that this is the oldest zircon age population in these samples. All three of these samples occur north of the Charles River Thrust and thus in the Aileron Province. For samples RBN-57, -61, -67, -68 and -71, the *c*. 1640 Ma age is interpreted as either metamorphic (reworking) or recrystallization of magmatic zircon, as the older *c*. 1760 Ma age population occurs in all these samples. In addition, Th/U plots for these samples (Figure 15) distinguish *c*. 1640 Ma metamorphic/recrystallised zircon (low Th/U) from older, igneous (higher Th/U) zircon .

The youngest population, delineated at *c.* 1135 Ma from sample HCSS, occurs mostly as rims, but also in zircon grains that can be identified as metamorphic from their internal structure. This timeline is uncommon in the zircon dataset, which is probably a function of; 1) rims typically too narrow to analyse; and/or 2) zircon dissolution and (re)growth appears to be only minimal during this event, as magmatism, at least at the current exposure level, does not seem to be abundant. This low amount of zircon dissolution and (re)growth could indicate that temperatures were too low during the Grenvillian-aged event for significant zircon dissolution to occur for either thermal and/or kinetic reasons (e.g. Watson & Harrison 1983; Watson 1996; Kelsey *et al*. 2008). The Grenvillian-aged zircons in all rock samples are interpreted to reflect reworking rather than magmatic ages, and this is strongly supported by low Th/U ratios (Figure 15) in all relevant samples (AS2012-1, 2, RBN-57, -68 and -71; Rubatto *et al*. 2001)

7.1.3 MAXIMUM DEPOSITIONAL AGE OF METASEDIMENTS

Detrital zircon analysis was undertaken on RBN-18, from within an unnamed Palaeoproterozoic gneissic unit of the Illyabba Metamorphics. The sample contains zircon with well-defined oscillatory zoning likely to record magmatism (Corfu *et al.* 2003). The maximum depositional age derived from the youngest and most significant peak of the

dataset, and exhibiting characteristic igneous morphologies, gives a weighted average $^{207}Pb/^{206}Pb$ age of 1819 ± 13 Ma (*n*=21, MSWD=1.7; Figure 14b). However, a more conservative maximum depositional age of *c*. 1770 Ma must be considered, due to the presence of several grains of this age. Comparably, Wong (2011) obtained conservative $^{207}Pb/^{206}Pb$ weighted average maximum depositional ages of 1823 ± 10 Ma (*n*=43, MSWD=2.7) and 1835 ± 20 Ma (*n*=23, MSWD=3.1) for metasedimentary samples located approximately 40 km to the east, near the Stuart Highway.

7.2 Spatial Distribution of Ages & Timelines

Tectonic events between *c.* 1070-1780 Ma have been recorded throughout the southern Aileron and northern Warumpi Provinces. The spatial distribution of samples and a summary of the monazite and/or zircon ages are presented in Figure 16 & Table 4 with U-Pb monazite or zircon ages from additional relevant studies in the southern Arunta region. It can be seen that the *c.* 1740-1780 Ma magmatic age population is spatially distributed to the north and south of the postulated boundary between the Aileron and Warumpi Provinces. This age population has been considered to be isolated to, and indicative of, the Aileron Province (Scrimgeour 2003a, Scrimgeour *et al.* 2005b, Claoue-Long *et al.* 2008). Similarly, the *c.* 1640 Ma age population, which has been considered to be isolated to the Warumpi Province, occurs to the north of the proposed boundary between the Warumpi and Aileron Provinces. On this basis, it appears that the Warumpi and Aileron Provinces have a shared tectonic history for these timelines, which casts doubt on the interpretation that the Warumpi Province is exotic to the Aileron Province (cf. Scrimgeour *et al.* 2005). This notion is supported by the presence of detrital zircon ages in the Warumpi Province that are similar to ages in the Aileron Province (Cross *et al.* 2004, Smits 2012).

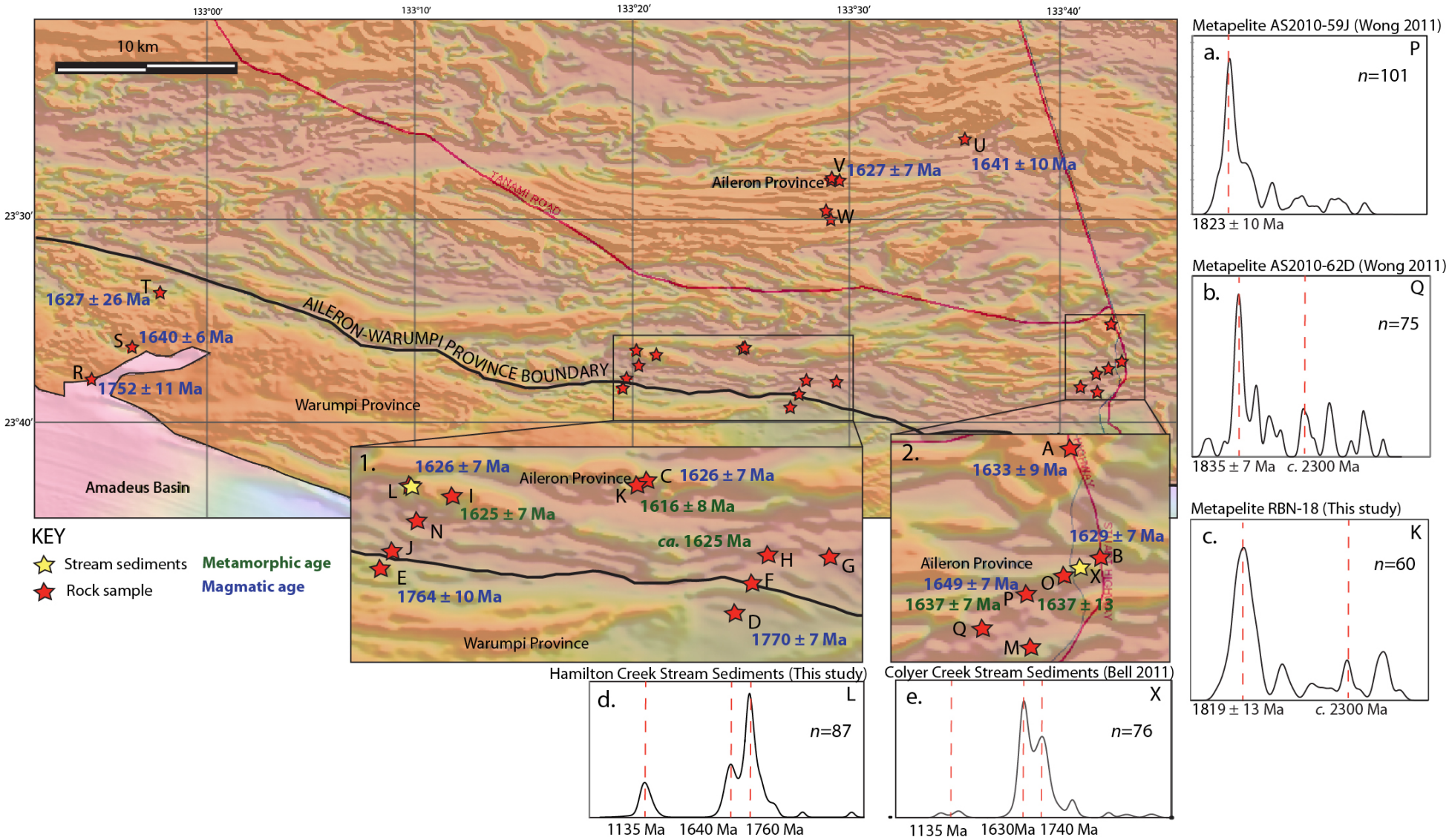

Figure 16: Spatial distribution of geochronological data collected from the southern Aileron and Warumpi Provinces shown against a TMI image to highlight the regional structure. For the full set of data provided to complement this study, including Wong (2011), Smits (2012) and Lawson-Wyatt (2012), see Table 4. Liebig-aged (*c.* 1630-1640 Ma) metamorphic (green) and magmatic (purple) ages are distributed either side of the proposed Aileron/Warumpi Province boundary. Rock samples collected in the field are depicted by a red star, and sample points for stream sediments are depicted by a yellow star. Age spectra plots (a) and (b) display the detrital ages for metasediments dated by Wong (2011) and detrital ages for RBN-18 is shown in (c). Age spectra plots display the distribution of ages from both modern stream sediment studies, (d) HCSS (L, this study, study area 1) and (e) Colyer Creek (X, Bell 2012, study area 2).

Table 4: A comparison of regional geochronological data correlating to the ages presented in this study; i.e. *c*. 1070-1150 Ma, *c*. 1630-1640 Ma and *c*. 1740-1780 Ma (see Figure 16).

	Study	Sample	Province	Geochronology Method	Event Type	Age (Ma)
A	This study	AS2012-1	Aileron	Zircon	Magmatism	1633 ± 9
B		AS2012-2	Aileron	Zircon	Metamorphism	1152 ± 34
					Magmatism	1629 ± 7
C		RBN-20	Aileron	Zircon	Magmatism	1626 ± 7
D		RBN-44	Warumpi	Monazite	Metamorphism	1071 ± 15
				Zircon	Magmatism	1770 ± 7
D		RBN-43	Warumpi	Monazite	Metamorphism	1074 ± 14
E		RBN-54	Warumpi	Monazite	Metamorphism	1096 ± 10
				Zircon	Magmatism	1764 ± 10
F		RBN-67	Warumpi/Aileron	Monazite	Metamorphism	1124 ± 10
				Zircon	Magmatism	*c.*1760
G		RBN-71	Aileron	Monazite	Metamorphism	1125 ± 10
				Zircon	Magmatism	*c.* 1780
H		RBN-68	Aileron	Monazite	Metamorphism	*c.* 1175
				Zircon	Metamorphism	1164 ± 19
				Monazite	Metamorphism	*c.* 1625
				Zircon	Magmatism	*c.* 1770
I		RBN-61	Aileron	Monazite	Metamorphism	1625 ± 7
				Zircon	Magmatism	1739 ± 9
J		RBN-57	Aileron	Zircon	Magmatism	1747 ± 6
K		RBN-18	Aileron	Monazite	Metamorphism	1616 ± 8
				Zircon	Maximum deposition	1819 ± 13
L		HCSS	Aileron/Warumpi	Zircon	Modern detritus	*c.* 1135
						c. 1640
						c. 1760
M	Wong (2012)	AS2010-66D	Aileron	Monazite	Metamorphism	1092 ± 5
						1720 ± 17
N		HAM2011-02	Aileron	Zircon	Metamorphism	1137 ± 8
L		HAM2011-08	Aileron	Zircon	Metamorphism	1139 ± 19
					Magmatism	1626 ± 7
O		COL2011-01	Aileron	Zircon	Metamorphism	1637 ± 7
O		AS2010-64J	Aileron	Zircon	Metamorphism	1637 ± 13
					Magmatism	1649 ± 7
P		AS2010-59J	Aileron	Zircon	Maximum deposition	1823 ± 10
Q		AS2010-62D	Aileron	Zircon	Maximum deposition	1835 ± 20
R	Smit (2012)	NAC-2011-016	Warumpi	Zircon	Magmatism	1752 ± 11
S		NAC-2011-019	Warumpi	Zircon	Magmatism	1640 ± 6
T		NAC-2011-033	Warumpi	Zircon	Magmatism	1627 ± 26
U	Lawson-Wyatt (2012)	RBN-34	Aileron	Zircon	Magmatism	1641 ± 10
V		RBN-45	Aileron	Zircon	Magmatism	1627 ± 7
				Monazite	Metamorphism	1754 ± 10
V		RBN-12	Aileron	Monazite	Metamorphism	1750 ± 8
V		RBN-47	Aileron	Monazite	Metamorphism	1744 ± 9
V		RBN-11	Aileron	Monazite	Metamorphism	1743 ± 11
W		RBN-26	Aileron	Monazite	Metamorphism	1745 ± 6
W		RBN-28	Aileron	Monazite	Metamorphism	1741 ± 7
W		RBN-31	Aileron	Monazite	Metamorphism	1750 ± 8
X	Bell (2011)	Colyer Creek	Aileron/Warumpi	Zircon	Modern detritus	*c.* 1135
					Modern detritus	*c.* 1640
					Modern detritus	*c.* 1760
					Modern detritus	*c.* 1940

The ages of monazite and zircon preserved in seven structurally constrained samples (see Table 2) within the study area range from 1739 ± 9 Ma (sample RBN-61) to *c.* 1780 Ma (RBN-71) and regionally correlate to the Inkamulla and Yambah events (see Table 1). The Yambah Event (*c* 1780-1770 Ma) has historically been characterised by felsic and less abundant mafic magmatism, and variable metamorphism widespread throughout the Arunta region (Collins *et al.* 1995, Young *et al.* 1995, Zhao & Bennett 1995, Scrimgeour 2003a, Claoué-Long & Hoatson 2005). Evidence for Inkamulla-aged, granitic and minor mafic magmatism is restricted to the southern and eastern Arunta region (Scrimgeour 2003a) and appears to reflect a southward contraction in the timing of magmatism, as magmatism of this age was not seen elsewhere throughout the Arunta region (Claoue-Long *et al.* 2008). Additionally, the earliest, dated tectonism within the Warumpi Province is the 1680-1660 Ma Argilke Event, characterised by felsic magmatism in the Haasts Bluff Domain (Scrimgeour 2003a, Close *et al*. 2004). However, this study and Smits (2012) provides evidence of Inkamulla/Yambah-aged magmatism in the Warumpi Province.

Similarly, igneous and metamorphic ages obtained from monazite and zircon preserved in six structurally constrained samples (Table 2) range from 1616 ± 8 Ma (sample RBN-18) to 1633± 9 Ma (AS2012-1) and regionally correlate to the Ormiston Igneous Event and Liebig Orogeny (see Table 1). The Ormiston Igneous Event (1615-1600 Ma) correlates with the metamorphic monazite age preserved in RBN-18; this event is currently believed to involve only minor felsic magmatism in the Warumpi Province (Collins *et al*. 1995, Zhao and McCulloch 1995, Scrimgeour 2003a). The metamorphic ages recorded in RBN-18, -61 & -68, combined with the three magmatic protolith ages of AS2012-1, -2, and RBN-20 as well as data from Wong (2011) and Lawson-Wyatt (2012), all distributed within the southern Aileron Province, shows further evidence that the effects of the Liebig Orogeny were not restricted to the Warumpi Province.

In support of Wong (2011) and Morrissey *et al*. (2011), the *c.* 1175-1070 Ma timeline preserved in eight samples in this study further emphasises the significance of the regional scale deformation attributed to the Teapot Thermal Event and its structural magnitude; as the crustal-scale high strain belts along the southern margin of the Aileron Province and northern margin of the Warumpi Province are Grenvillian. Additionally, both low-strain samples RBN-18 and RBN-61 solely exhibiting 1616 and 1625 Ma deformation ages respectively, with no evidence of Grenvillian overprint, make a case for the age of the low-strain domains within the E-W high strain belt.

Wong (2011) found evidence in granulite facies rock for Chewings aged monazites; however, this was evident in only one sample. Curiously, no Chewings-aged (1590-1560 Ma) data was obtained during this study. However, Lawson-Wyatt (2012) found evidence for *c*. 1550-1590 Ma (early Mesoproterozoic) deformation in U-Pb monazite data further north in the southern Aileron Province, which supports the presence of localised Chewings-aged deformation in the southern Aileron Province.

The metapelitic sample RBN-18, from within the Illyabba Metamorphics, is a crucial sample as it provides information about the tectonothermal regime at the time it was metamorphosed. It preserves a monazite metamorphic age of 1616 ± 8 Ma, and *P-T* conditions of 740–900 °C, 7-8 kbar. This P-T field spans 260 °C (Figure 7), and thus the conditions are difficult to constrain to a specific geothermal gradient. However, this evidence can be interpreted that RBN-18 evolved through a down-pressure *P-T* history. Elemental X-ray maps of garnet showed Mn-enrichment at the edges of the grains, suggestive of garnet consumed during metamorphism (Figure 6). Textural evidence of this is also observed; cordierite in direct contact and partially surrounding garnet could plausibly suggest partial resorption of garnet, and possibly records decompressional production of cordierite coronae (Figure 5). Down-

pressure *P-T* histories, coupled with the development of low angle tectonic fabrics, are features commonly observed in extensional terranes.

Another feature of the metapelitic sample RBN-18 is the presence of a *c.* 2300 detritus peak (Figure 14e, 16c). This feature is also observed in detrital U-Pb data collected by Wong (2011, Aileron Province; Figure 16a-b), Howlett (2012, Aileron Province), Lawson-Wyatt (2012, Aileron Province), Reid (2012, Aileron Province), Smits (2012, Warumpi Province) and in published data by Claoue-Long *et al.* (2008, Aileron Province) and Cross *et al.*(2003, Warumpi Province). The source region/event corresponding to this peak is unclear; however its presence in a number of samples in the NAC is intriguing, as this timeline is recognised globally as a time of rare zircon growth (Condie *et al.* 2009, Condie *et al.* 2011, Voice *et al.* 2011). The presence of these unusual aged detrital zircons in both provinces suggests they may share a common history.

The modern stream sediment analysis obtained in HCSS at Hamilton Creek has a similar distribution of ages to the data collected by Bell (2012) from Colyer Creek which drains country to the east of the study area (Figure 16d-e). Both samples display three main peaks, at *c.* 1135 Ma, *c*. 1635 and *c*. 1750 Ma. Two metapelite samples dated by Wong (2011), presumably zircon sources for Colyer Creek, are both lacking in *c*. 1750 Ma and *c*. 1630 Ma detrital peaks, suggesting the stream sediments are dominated by the igneous rocks of the drainage area. Furthermore, a Th/U vs. age plot for HCSS (figure 15c) highlights that the stream sediments in Hamilton Creek, which drains the Warumpi Province, are dominated by zircon of magmatic origin, also suggesting igneous rocks in the drainage area are the primary source of 1750 Ma and 1640 Ma zircon.

7.3 Regional Implications

Extensive monazite and zircon geochronological data collected from structurally constrained samples throughout the southern Aileron and Warumpi provinces has provided new insight for the geological history of the southern Arunta region. The only recent authors to have discussed the temporal framework are Scrimgeour *et al*. (2005b), Morrisey (2011) and Wong (2011); the key implication of the work of Scrimgeour *op cit.* is the exotic nature of the Warumpi Province based on 1690-1600 Ma sedimentary and igneous protolith ages (Close *et al.* 2004, Scrimgeour *et al.* 2005b) believed to be part of a terrane that is exotic to the Aileron Province. However, this study combined with Wong (2011) and Lawson-Wyatt (2012) provides convincing evidence of *c.* 1630-1650 Ma magmatism within the southern Aileron Province. The only scenario that supports the suggestion of Scrimgeour *et al*. (2005b) is the emplacement of magmas occurring syn-tectonically with the collision of the Warumpi and Aileron Provinces; however, in that case, the southernmost edge of the Aileron Province should record *c*. 1640 Ma metamorphism and deformation. The age data obtained by Lawson-Wyatt (2012) from the immediately adjacent rocks in the Aileron Province did not find evidence for this.

A speculative interpretation of this study is that the Liebig-aged metamorphism and magmatism, seemingly associated with low angle/low strain fabrics and coupled with the *c.* 1635 Ma Andrew Young Hills mafic intrusion (Young *et al.* 1995, Claoué-Long & Hoatson 2005), all located within the Aileron Province, provides a better case for the Liebig Orogeny as an extensional event, that deformed the Aileron Province lithosphere. Considering an extensional system raises the possibility that the 1640-1615 Ma magmatism and metamorphism recorded in the Warumpi and southern Aileron Provinces occupied a lower plate position in an extensional regime, with sedimentary units (i.e. Simpsons Gap Metasediments and Chewings Range Quartzite) being an upper plate basinal succession.

Through the extensional process at ~1630 Ma, with the hanging wall plate being drawn down while the footwall moves up, this process of progressive structural juxtaposition results in a structure that would have exhumed a metamorphic footwall juxtaposed against the unmetamorphosed sedimentary succession separated by a large extensional detachment system.

Deposition of the Iwupataka Metamorphic Complex sediments i.e. Simpsons Gap Metasediments and Chewings Range Quartzite is postulated to occur ~1620–1610 Ma (Cross *et al.* 2004). However, there is nothing available in the existing geochronological data that does not preclude the metasediments of the Iwupataka Metamorphic assemblage being syn-tectonically deposited at between ~1630–1615 Ma, concident with the magmatism and metamorphism recorded in this study. The intrusion of the Burts Bluff Gneiss (1603 ± 7 Ma, Zhao and Bennett 1995) only provides a minimum depositional age of the Simpsons Gap Metasediments, which does not rule out the extensional scenario (figure 17).

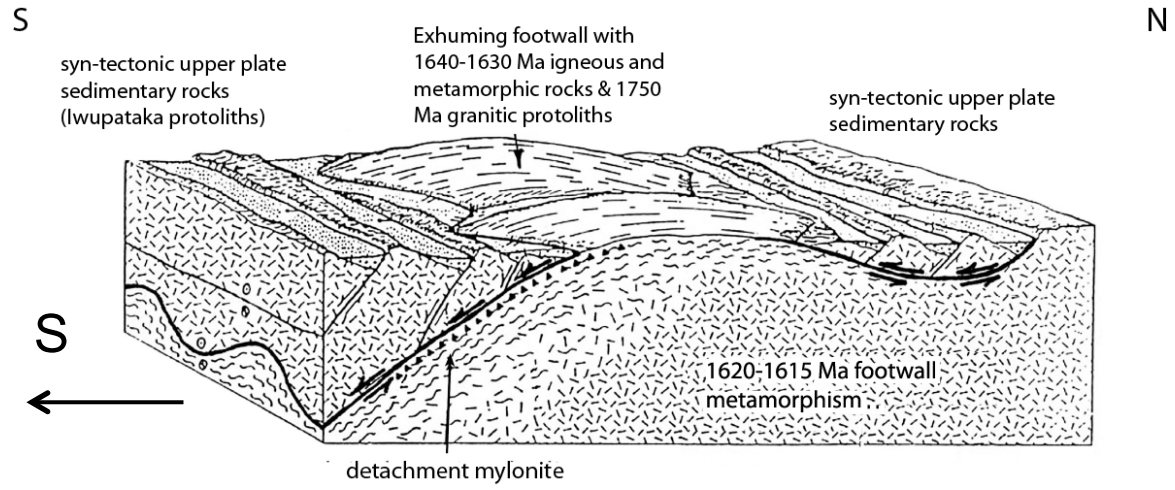

Figure 17: Schematic demonstrating the postulated extensional tectonic setting at *c*. 1615 Ma (adapted from Spencer and Reynolds 1991).

There remains a number of unanswered questions about the Palaeo- and Meso- Proterozoic tectonic setting and geodynamic significance of the Warumpi Province and southern margin

of the Aileron Province. For example, is the Warumpi Province simply a region of extended Aileron Province, with younger magmatism and sedimentation reflecting the extension? The fundamental reason for this continuing ambiguity is the paucity of data from the southern Arunta region, despite the vast and often exceptional outcrop exposure. By collecting an extensive geochronological data set, integrated with field structural observations, geophysical imagery, *P-T* data, mineral compositional data, previously published work and new data from concurrently running projects, this project has attempted to address this significant issue. New constraints have shed more light on the tectonics of the Arunta region, an area of the North Australian Craton believed to be crucial to understanding the growth and assembly of the Australian continent during the Proterozoic.

8 CONCLUSION

U-Pb geochronology in the southern Arunta region has shown it is characterised by *c.* 1780-1740 Ma magmatic rocks and *c*. 1640-1615 Ma magmatic and metamorphic rocks. The evidence for these events is preserved in kilometre-scale migmatitic boudins and low-strain zones enveloped by pervasive E-W trending higher strain belts. The overprinting high strain fabrics are Grenvillian age and constrained to *c*. 1175-1070 Ma. Phase equilibria modelling on a metapelite from a low-strain domain within the southern Aileron Province indicates peak metamorphic conditions were ~7-8 kbar and between 740-900 °C and associated with a down-pressure or decompressional P-T history. The older, low-strain domains also preserve a *c*. 1620 Ma age in a granitic gneiss and a metapelite. The presence of the *c.* 1760 Ma and *c.* 1640 Ma timelines in both the Warumpi and Aileron Provinces calls into question the proposed exotic nature of the Warumpi Province. A speculative interpretation is that the Liebig-aged metamorphism and magmatism, seemingly associated with relatively shallow orientated, low strain fabrics, represents a period of extension rather than collision.

9 ACKNOWLEDGMENTS

First and foremost, I am most thankful to my primary supervisors, David Kelsey, Martin Hand and Justin Payne for their unwavering support and guidance throughout the year. I couldn't have asked for a more enjoyable experience during my Honours degree, I value each of you for your insight and individual contributions to my project. I feel very privileged to have worked alongside all of you. Thank you to the postgraduates of the Continental Evolution Research Group – Jade Anderson, Russell Smits, Laura Morrissey, Bonnie Henderson and Kathleen Lane. A special thanks to Alec Walsh, for his work with Theriak-Domino, it is much appreciated. Katie Howard, for being a fantastic Honours Support Officer and friend. A huge thank you to Angus Netting, Ben Wade and Aoife McFadden at Adelaide Microscopy. I must thank Belinda Wong for her continued interest and support during the year. Of course, to the 'Centrals Group', Mathew Reid, Daniel Howlett, Maddison Lawson-Wyatt and Claire Thomas, it was fantastic to share this experience with you. Lastly, to my dear friends and family who have stood by me through the year, I wouldn't have made it through without you. This project was funded by ARC discovery project DP1095456 and ARC linkage project LP100200127.

10 REFERENCES

BELL J. 2012. Detrital zircon analysis on the geological evolution of the southern Arunta orogen. BSc Hons (unpub) thesis, University of Newcastle (unpubl.).

BETTS P. G. & GILES D. 2006. The 1800-1100 Ma tectonic evolution of Australia. *Precambrian Research* **144**, 92-125.

BETTS P. G., GILES D., LISTER G. S. & FRICK L. R. 2002. Evolution of the Australian lithosphere. *Australian Journal of Earth Sciences* **49**, 661-695.

BETTS P. G., GILES D. & SCHAEFER B. F. 2008. Comparing 1800-1600 Ma accretionary and basin processes in Australia and Laurentia: Possible geographic connections in Columbia. *Precambrian Research* **166**, 81-92.

BIERMEIER C., STÜWE K., FOSTER D. A. & FINGER F. 2003. Thermal evolution of the Redbank thrust system, central Australia: Geochronological and phase-equilibrium constraints. *Tectonics* **22**, 1-23.

BUICK I. S. & CARTWRIGHT I. 1996. Fluid—Rock Interaction during Low-Pressure Polymetamorphism of the Reynolds Range Group, Central Australia. *Journal of Petrology* **37**, 1097-1124.

CARSON C. J., CLAOUÉ-LONG G. J., STERN R. A., CLOSE D. F., SCRIMGEOUR I. R. & GLASS L. M. 2009. *Summary of results. Joint NTGS-GS geochronology project: Arunta and Pine Creek regions, July 2006-May 2007*. Survey. N. T. G. **2009-001**, Darwin.

CAWOOD P. A. & KORSCH R. J. 2008. Assembling Australia: Proterozoic building of a continent. *Precambrian Research* **166**, 1-38.

CLAOUE-LONG J., EDGOOSE C. & WORDEN K. E. 2008. A correlation of Aileron Province stratigraphy in central Australia. *Precambrian Research* **166**, 230-245.

CLAOUÉ-LONG J. & EDGOOSE C. J. 2008. The age and significance of the Ngadarunga Granite in Proterozoic central Australia. *Precambrian Research* **166**, 219-229.

CLAOUÉ-LONG J. & HOATSON D. M. 2005. Proterozoic mafic-ultramafic intrusions in the Arunta Region, central Australia. Part 2: Event chronology and regional correlations. *Precambrian Research* **142**, 134-158.

CLARKE G. L. & POWELL R. 1991. Decompressional coronas and symplectites in granulites of the Musgrave Complex, central Australia. *Journal of Metamorphic Geology* **9**, 441-450.

CLOSE D., SCRIMGEOUR I., EDGOOSE C., FRATER M. & CROSS A. 2004. New insights into geology and prospectivity of the southwestern Arunta Region, p. 37.

COGGON R. & HOLLAND T. J. B. 2002. Mixing properties of phengitic micas and revised garnet-phengite thermobarometers. *Journal of Metamorphic Geology* **20**, 683-696.

COLLINS W. J. & SHAW R. D. 1995. Geochronological constraints on orogenic events in the Arunta Inlier; a review. *Precambrian Research* **71**, 315-346.

COLLINS W. J. & VERNON R. H. 1991. Orogeny associated with anticlockwise P-T-t paths; evidence from low-P, high-T metamorphic terranes in the Arunta Inlier, central Australia. *Geology Boulder* **19**, 835-838.

COLLINS W. J., WILLIAMS I. S., SHAW R. D. & MCLAUGHLIN N. A. 1995. The age of the Ormiston Pound Granite: implications for Mesoproterozoic evolution of the Arunta Inlier, central Australia. *Precambrian Research* **71**.

CONDIE K. C., BELOUSOVA E., GRIFFIN W. L. & SIRCOMBE K. N. 2009. Granitoid events in space and time: Constraints from igneous and detrital zircon age spectra. *Gondwana Research* **15**, 228-242.

CONDIE K. C., BICKFORD M., ASTER R. C., BELOUSOVA E. & SCHOLL D. W. 2011. Episodic zircon ages, Hf isotopic composition, and the preservation rate of continental crust. *Geological Society of America Bulletin* **123**, 951-957.

CORFU F., HANCHAR J. M., HOSKIN P. W. O. & KINNY P. 2003. Atlas of Zircon Textures. *Reviews in Mineralogy and Geochemistry* **53**, 469-500.

CROSS A., CLAOUÉ-LONG J., SCRIMGEOUR I. R., CLOSE D. F. & EDGOOSE C. J. 2004. Summary of results. Joint NTGS-GA geochronology project southern Arunta region. *NTGS Record 2004-03*.

CROSS A., CLAOUÉ-LONG J. C. & CRISPE A. J. 2003. *Summary of Results. Joint NTGS – GA geochronology project: Tanami region 2001-2002.* Survey N. T. G. **2003-006**, Darwin.

DE CAPITANI C. & PETRAKAKIS K. 2010. The computation of equilibrium assemblage diagrams with Theriak/Domino software. *American Mineralogist* **95**, 1006-1016.

DIENER J. F. A., POWELL R., WHITE R. W. & HOLLAND T. J. B. 2007. A new thermodynamic model for clino- and orthoamphiboles in the system Na2O–CaO–FeO–MgO–Al2O3–SiO2–H2O–O. *Journal of Metamorphic Geology* **25**, 631-656.

DIRKS P. H. G. M., HAND M. & POWELL R. 1991. The P-T-deformation path for a mid-Proterozoic, low-pressure terrane; the Reynolds Range, central Australia. *Journal of Metamorphic Geology* **9**, 641-661.

DIRKS P. H. G. M. & WILSON C. J. L. 1990. The geological evolution of the Reynolds Range, central Australia; evidence for three district structural-metamorphic cycles. *Journal of Structural Geology* **12**, 651-665.

FLÖTTMANN T. & HAND M. 1999. Folded basement-cored tectonic wedges along the northern edge of the Amadeus Basin, central Australia: evaluation of orogenic shortening. *Journal of Structural Geology* **21**.

GILES D., BETTS P. G. & LISTER G. S. 2002. Far-field continental backarc setting for the 1.80-1.67Ga basins of northeastern Australia. *Geology*.

GILES D., BETTS P. G. & LISTER G. S. 2004. 1.8-1.5-Ga links between the North and South Australian Cratons and the Early-Middle Proterozoic configuration of Australia. *Tectonophysics* **380**, 27-41.

GOLEBY B. R., SHAW R. D., WRIGHT C., KENNETT B. L. N. & LAMBECK K. 1989. Geophysical evidence for "thick-skinned" crustal deformation in central Australia. *Nature London* **337**, 325-330.

GOSCOMBE B. 1992. High-Grade Reworking of Central Australian Granulites: Metamorphic Evolution of the Arunta Complex. *Journal of Petrology* **33**, 917-962.

GREEN E., HOLLAND T. & POWELL R. 2007. An order-disorder model for omphacitic pyroxenes in the system jadeite-diopside-hedenbergite-acmite, with applications to eclogitic rocks. *American Mineralogist* **92**, 1181-1189.

GREENFIELD J. E., CLARKE G. L. & WHITE R. W. 1998. A sequence of partial melting reactions at Mt Stafford, central Australia. *Journal of Metamorphic Geology* **16**, 363-378.

GRIFFIN W. L., POWELL W. J., PEARSON N. J. & O'REILLY S. Y. 2008. *GLITTER: data reduction software for laser ablation ICP-MS. Laser Ablation ICP-MS in the Earth Sciences: Current Practices and Outstanding Issues., Mineralogical Association of Canada. Short Course Series 40*. Sylvester P.**:** 308-311.

HAINES P. W., HAND M. & SANDIFORD M. 2001. Palaeozoic synorogenic sedimentation in central and northern Australia: a review of distribution and timing with implications for the evolution of intracontinental orogens. *Australian Journal of Earth Sciences* **48**, 911-928.

HAND M. & BUICK I. S. 2001. The tectonic evolution of the Reynolds-Anmatjira Ranges: a case study in terrain reworking from the Arunta Inlier, central Australia. *Geological Society of London, Special Publications* **184**, 237-260.

HAND M., MAWBY J. O., KINNY P. D. & FODEN J. 1999. U–Pb ages from the Harts Range, central Australia: evidence for early Ordovician extension and constraints on Carboniferous metamorphism. *Journal of the Geological Society* **156**, 715-730.

HOATSON D. M., SUN S. & CLAOUÉ-LONG J. 2005. Proterozoic mafic-ultramafic intrusions in the Arunta Region, central Australia. Part 1: Geological setting and mineral potential. *Precambrian Research* **142**, 93-133.

HOLLAND T. & POWELL R. 2003. Activity–composition relations for phases in petrological calculations: an asymmetric multicomponent formulation. *Contributions to Mineralogy and Petrology* **145**, 492-501.

HOLLAND T. J. B. & POWELL R. 1998. An internally consistent thermodynamic dataset for phases of petrological interest. *Journal of Metamorphic Geology* **16**, 309-343.

HOWLETT D. P. 2012. Geochronological constraints on Yambah and Chewings aged deformation at Mt Boothby in the south eastern Reynolds Range, central Australia. BSc. (Honours) thesis, Geology and Geophysics, University of Adelaide, Adelaide (unpubl.).

JACKSON M. J., PEARSON N. J., GRIFFIN W. L. & BELOUSOVA E. A. 2004. The application of laser ablation-inductively coupled plasma-mass spectrometry to in situ U-Pb zircon geochronology. *Chemical Geology* **211**, 47-69.

KELLY N. M., CLARKE G. L. & HARLEY S. L. 2006. Monazite behaviour and age significance in poly-metamorphic high-grade terrains: A case study from the western Musgrave Block, central Australia. *Lithos* **88**, 100-134.

KELSEY D. E., CLARK C. & HAND M. 2008. Thermobarometric modelling of zircon and monazite growth in melt-bearing systems: examples using model metapelitic and metapsammitic granulites. *Journal of Metamorphic Geology* **26**, 199-212.

KELSEY D. E., POWELL R., WILSON C. J. L. & STEELE D. A. 2003. (Th+U)-Pb monazite ages from Al-Mg-rich metapelites, Rauer Group, east Antarctica. *Contributions to Mineral Petrology* **146**, 326-340.

KINGSBURY J. A., MILLER C. F., WOODEN J. L. & HARRISON T. M. 1993. Monazite paragenesis and U-Pb systematics in rocks of the eastern Mojave Desert, California, USA.: implications for thermochronometry. *Chemical Geology* **110**, 147-167.

KORSCH R. J., GOLEBY B. R., LEVEN J. H. & DRUMMOND B. J. 1998. Crustal architecture of central Australia based on deep seismic reflection profiling. *Tectonophysics* **288**, 57-69.

LAMBECK K., BURGESS G. & SHAW R. D. 1988. Teleseismic travel-time anomalies and deep crustal structure in central Australia. *Geophysical Journal* **94**.

LAWSON-WYATT M. 2012. Regional Inkamulla-aged (ca. 1740-1755 Ma) tectonism along strike of the Mt. Hay-Redbank Hill region, southern Aileron Province, central Australia. B.Sc (Honours) thesis, Geology and Geophysics, University of Adelaide, Adelaide (unpubl.).

LUDWIG K. R. 2003. User's Manual for Isoplot 3.00. *Berkeley Geochronological Centre, Special Publication*.

MAIDMENT D., HAND M. & WILLIAMS I. S. 2005. Tectonic cycles in the Strangways Metamorphic Complex, Arunta Inlier, central Australia: geochronological evidence for exhumation and basin formation between two high-grade metamorphic events. *Australian Journal of Earth Sciences* **52**, 205-215.

MAWBY, HAND & FODEN 1999. Sm–Nd evidence for high-grade Ordovician metamorphism in the Arunta Block, central Australia. *Journal of Metamorphic Geology* **17**, 653-668.

MORRISSEY L., PAYNE J. L., KELSEY D. E. & HAND M. 2011. Grenvillian-aged reworking in the North Australian Craton, central Australia: constraints from geochronology and modelled phase equilibria. *Precambrian Research* **191**.

MYERS J. S., SHAW R. D. & TYLER I. M. 1996. Tectonic evolution of Proterozoic Australia. *Tectonics* **15**, 1431-1446.

NORMAN A. R. & CLARKE G. L. 1990. A barometric response to late compression in the Strangways Metamorphic Complex, Arunta Block, central Australia. *Journal of Structural Geology* **12**, 667-684.

NORTHERN TERRITORY GEOLOGICAL SURVEY 2012. Strike NTGS <http://geoscience.nt.gov.au/GeosambaU/strike_gs_webclient/default.aspx>. (retrieved 16/07/2012 2012).

OFFE L. A. & SHAW R. D. 1983. Alice Springs Region, Northern Territory. 1:100 000 Map Commentary. *Bureau of mineral resources, Geology and Geophysics*.

PAYNE J. L., FERRIS G., BAROVICH K. M. & HAND M. 2010a. Pitfalls of classifying ancient magmatic suites with tectonic discrimination diagrams: An example from the Paleoproterozoic Tunkillia Suite, southern Australia. *Precambrian Research* **177**, 227-240.

PAYNE J. L., FERRIS G., BAROVICH K. M. & HAND M. 2010b. Pitfalls of classifying ancient magmatic suites with tectonic discrimination diagrams: An example from the Paleoproterozoic Tunkillia Suite, southern Australia. *Precambrian Research* **177**, 227-240.

PAYNE J. L., HAND M., BAROVICH K. M., REID A. & EVANS D. A. D. 2009. Correlations and reconstruction models for the 2500-1500 Ma evolution of the Mawson Continent. *Geological Society of London, Special Publications* **323**, 319-355.

PAYNE J. L., HAND M., BAROVICH K. M. & WADE B. P. 2008. Temporal constraints on the timing of high-grade metamorphism in the northern Gawler Craton; implications for assembly of the Australian Proterozoic. *Australian Journal of Earth Sciences* **55**, 623-640.

REID M. D. 2012. New constraints on Chewings-aged deformation and metamorphism of ca.≥ 1750 Ma crust in the Reynolds Range,central Australia. B.Sc (Honours) thesis, Geology and Geophysics, University of Adelaide, Adelaide (unpubl.).

RUBATTO D., WILLIAMS I. S. & BUICK I. S. 2001. Zircon and monazite response to prograde metamorphism in the Reynolds Range, central Australia. *Contrib Mineral Petrol* **140**, 458-468.

SANDIFORD M. & HAND M. 1998. Controls on the locus of intraplate deformation in central Australia. *Earth and Planetary Science Letters* **162**, 97-110.

SCOTT D. L., RAWLINGS D. J., PAGE R. W., TARLOWSKI C. Z., IDNURM M., JACKSON M. J. & SOUTHGATE P. N. 2000. Basement framework and geodynamic evolution of the Palaeoproterozoic superbasins of north-central Australia: an integrated review of geochemical, geochronological and geophysical data. *Australian Journal of Earth Sciences* **47**, 341-380.

SCRIMGEOUR I. 2003a. Developing a revised framework for the Arunta region. *Geological Survey Record* **001**, 2003-2001.

SCRIMGEOUR I. R. 2003b. Developing a revised framework for the Arunta Region. In Annual Geoscience Exploration Seminar (AGES). *Record of Abstracts, Northern Territory Geological Survey Record 2003-001*.

SCRIMGEOUR I. R., CLOSE D. F. & EDGOOSE C. J. 2005a. Mount Leibig Northern Territory (second ed.) 1:250 000 geological map series explanatory notes. *Northern Territory Geological Survey, Darwin.*

SCRIMGEOUR I. R., KINNY P. D., CLOSE D. F. & EDGOOSE C. J. 2005b. High-T granulites and polymetamorphism in the southern Arunta Region, central Australia: Evidence for a 1.64 Ga accretional event. *Precambrian Research* **142**, 1-27.

SELWAY K., HAND M., HEINSON G. & PAYNE J. L. 2009. Magnetotelluric constraints on subduction polarity: Reversing reconstruction models for Proterozoic Australia. *Geology*.

SHAW R. D., ZEITLER P. K., MCDOUGALL I. & TINGATE P. R. 1992. The Paleozoic history of an unusual intracratonic thrust belt in central Australia based on 40Ar/39Ar, K-Ar and fission-track dating. *Journal of the Geological Society* **149**, 937-954.

SLÁMA J., KOŠLER J., CONDON D. J., CROWLEY J. L., GERDES A., HANCHAR J. M., HORSTWOOD S. A., MORRIS G. A., NASDALA L., NORBERG N., SCHALTEGGER U., SCHOENE B., TUBRETT M. N. & WHITEHOUSE M. J. 2008. Plešovice zircon- A new natural reference material for U-Pb and Hf isotopic microanalysis. *Chemical Geology* **249**, 1-35.

SMITHIES R. H., HOWARD H. M., EVINS P. M., KIRKLAND C., KELSEY D. E., HAND M., WINGATE M., T. D., COLLINS A. S. & BELOUSOVA E. A. 2011. High-temperature granite magmatism, crust-mantle interaction and the Mesoproterozoic intracontinental evolution of the Musgrave Province, central Australia. *Journal of Petrology* **52**, 931-958.

SMITS R. 2012. *in prep., October 2012. U-Pb zircon LA-ICP-MS dating, samples NAC-2011-016, NAC-2011-019 & NAC-2011-033.* Hand. University of Adelaide, Adelaide.

SPEAR F. S. 2004. Fast cooling and exhumation of the Valhalla metamorphic core complex, southeastern British Columbia. *International Geology Review* **46**, 193-209.

SPEAR F. S. & KOHN M. J. 1996. Trace element zoning in garnet as a monitor of crustal melting. *Geology* **24**, 1099-1102.

SPENCER J. E. & REYNOLDS S. J. 1991. Tectonics of mid-Tertiary extension along a transect through west central Arizona. *Tectonics* **10**, 1204-1221.

TEYSSIER C. 1985. A crustal system in an intracratonic tectonic environment. *Journal of Structural Geology* **7**, 689-700.

TEYSSIER C., AMRI C. & HOBBS B. E. 1988. South Arunta Block: The internal zones of a proterozoic overthrust in central Australia. *Precambrian Research* **40/41**, 157-173.

VOICE P. J., KOWALEWSKI M. & ERIKSSON K. A. 2011. Quantifying the Timing and Rate of Crustal Evolution: Global Compilation of Radiometrically Dated Detrital Zircon Grains. *The Journal of Geology* **119**, 109-126.

VRY J., COMPSTON W. & CARWRIGHT I. 1996. SHRIMP II dating of zircons and monazites: reassessing the timing of high-grade metamorphism and fluid flow in the Reynolds

Range, northern Arunta Block, Australia. *Journal of Metamorphic Geology* **14**, 335-350.

WADE B. P., BAROVICH K. M., HAND M., SCRIMGEOUR I. R. & CLOSE D. F. 2006. Evidence for Early Mesoproterozoic arc magmatism in the Musgrave Block, central Australia: Implications for Proterozoic crustal growth and tectonic reconstructions of Australia. *Geology*.

WARREN R. G. & SHAW R. D. 1995. Hermansburg, Northern Territory (second ed.) 1:250 000 geological map series explanatory notes. *Northern Territory Geological Survey, Darwin.*

WATSON E. B. 1996. Dissolution, growth and survival of zircons during crustal fusion: kinetic principals, geological models and implications for isotopic inheritance. *Earth and Environmental Science Transactions of the Royal Society of Edinburgh* **87**, 43-56.

WATSON E. B. & HARRISON T. M. 1983. Zircon saturation revisited: temperature and composition effects in a variety of crustal magma types. *Earth and Planetary Science Letters* **64**, 295-304.

WHITE, POWELL, HOLLAND & WORLEY 2000. The effect of TiO2 and Fe2O3 on metapelitic assemblages at greenschist and amphibolite facies conditions: mineral equilibria calculations in the system K2O–FeO–MgO–Al2O3–SiO2–H2O–TiO2–Fe2O3. *Journal of Metamorphic Geology* **18**, 497-511.

WHITE R. W., POWELL R. & CLARKE G. L. 2002. The interpretation of reaction textures in Fe-rich metapelitic granulites of the Musgrave Block, central Australia: constraints from mineral equilibria calculations in the system K2O–FeO–MgO–Al2O3–SiO2–H2O–TiO2–Fe2O3. *Journal of Metamorphic Geology* **20**, 41-55.

WHITE R. W., POWELL R. & HOLLAND T. J. B. 2007. Progress relating to calculation of partial melting equilibria for metapelites. *Journal of Metamorphic Geology* **25**, 511-527.

WONG B. L. 2011. Grenvillian-aged reworking of late Paleoproterozoic crust in the southern Aileron Province, central Australia: implications for the assembly of Mesoproterozoic Australia. Centre for Tectonics, Resources and Exploration, The University of Adelaide, South Australia, Adelaide (unpubl.).

YOUNG D. N., FANNING C. M., SHAW R. D., EDGOOSE C. J., BLAKE D. H., PAGE R. W. & CAMACHO A. 1995. U-Pb zircon dating of tectonomagmatic events in the northern Arunta Inlier, central Australia. *Precambrian Research* **71**, 45-68.

ZHAO J.-X. & BENNETT V. C. 1995. SHRIMP U-Pb zircon geochronology of granites in the Arunta Inlier, central Australia; implications for Proterozoic crustal evolution. *Precambrian Research* **71**, 17-43.

ZHAO J. 1994. Geochemical and Sm-Nd isotopic study of amphibolites in the southern Arunta Inlier, central Australia: evidence for subduction at a Proterozoic continental margin. *Precambrian Research* **65**, 71-94.

APPENDIX A: WHOLE ROCK GEOCHEMICAL ANALYSIS

Phase equilibria modelling was undertaken using the metapelitic sample RBN-18. Major element abundances (shown below) were determined by fusing the crushed/powdered sample with lithium metaborate before dissolution and analysis using ICP–MS (Payne *et al.* 2010a, Morrissey *et al.* 2011). REE abundances were determined by digesting the analytical pulp in a multi-acid HF solution before analysis using ICP–MS.

Major elements	**(wt%)**
SiO_2	50
TiO_2	1.15
Al_2O_3	26.4
Cr_2O_3	0.0245
Fe_2O_3	12.6
MnO	0.09
MgO	5.74
ZnO	0.01
CaO	0.33
Na_2O	0.25
K_2O	3.07
LOI	0.91
P_2O_5	0.02
Trace and REE	**(ppm)**
Cr	245
Zn	100.00
Sc	25
V	170
Ba	1060
Be	6
Hf	7
Sn	<10
Ta	<2
Trace & REE	**(ppm)**

cont.	
Zr	260
Cs	5.5
Ga	30.5
Mo	0.6
Nb	15
Rb	180
Sr	37.5
Th	37.5
U	3.3
Y	19.5
Zr	70
Ce	170
Dy	5
Er	2.6
Eu	1.6
Gd	9
Ho	0.92
La	90
Lu	0.36
Nd	70
Pr	19.5
Sm	11
Tb	1.05
Tm	0.25
Yb	1.8

APPENDIX B: PHASE EQUILIBRIA MODELLING METHOD

Major element anaylsis was obtained by fusion of a 0.1 g sub-sample of the analytical pulp with lithium metaborate, followed by dissolution in nitric acid solution to give a 'total solution' and finally analysed by Inductively Coupled Plasma-Optical Emission Spectroscopy (ICP-OES). Analysis of trace and REE elements is achieved by digestion of up to 0.5 g of the analytical pulp in a Hydrofluric/multi-acid solution and introduced into an Inductively Coupled Plasma-Mass Spectrometry for the quantification of the elements of interest (Payne *et al.* 2010b). ICP-OES and ICP-MS analyses were performed on a Perkin Elmer 5300 V and a Perkin Elmer ELAN 9000, respectively. H_2O content is based on loss on ignition during analysis. Analysis via titration methods provides the concentration of ferric iron. Due to the inevitable hydration and oxidation of the sample during retrogression and/or weathering at the surface, the H_2O and Fe_2O_3 values of the composition used for phase diagram calculations should be considered a maximum estimate.

The *P-T* pseudosection was calculated for the metapelitic sample RBN-18 (Figure 7) using the THERIAK-DOMINO program (de Capitani & Petrakakis 2010), for the geologically realistic chemical system SiO_2–Al_2O_3–FeO–Fe_2O_3–MgO–CaO–Na_2O–K_2O–H_2O–TiO_2 (NCKFMASHTO). The dataset used the following *a–x* models which incorporate Fe^{3+} end-member minerals: garnet, biotite and melt (White *et al.* 2007), muscovite (Coggon & Holland 2002), orthopyroxene and magnetite (White *et al.* 2002), amphibole (Diener *et al.* 2007), cordierite (Holland & Powell 1998), Clinopyroxene (Green *et al.* 2007), K-feldspar and plagioclase (Holland & Powell 2003) and ilmenite (White *et al.* 2000). Mn is not considered for the reasons given by White *et al*. (2007). Mineral abbreviations are as follows: g – garnet; cd – cordierite; sp – spinel; sill – sillimanite; bi – biotite; ksp – K-feldspar; ilm– ilmenite; mt – magnetite; q – quartz; liq – silicate liquid/melt. The Theriak–Domino software calculates

equilibrium mineral assemblages for a specific bulk-rock composition that minimises Gibbs-free energy at a given point in pressure–temperature space.

APPENDIX C: U-PB MONAZITE & ZIRCON LA-ICP-MS GEOCHRONOLOGY METHODS

U-Pb MONAZITE LA–ICP–MS GEOCHRONOLOGY

Monazite geochronology was undertaken on monazite grains that were separated from crushed rock. Monazite was extracted from whole rock samples of approximately 2 kg using a crusher, tungsten carbide mill and conventional sieving (to recover grains between 79µm and 400µm) followed by panning, Frantz Isodynamic magnetic and heavy liquid separation techniques. Individual monazite grains were then hand-picked, mounted in 2.5 cm diameter circular epoxy grain mounts and hand polished until the centre of the monazite was revealed. Prior to analysis, all monazite grains were imaged using a backscattered electron (BSE) detector on a Phillips XL30 Scanning Electron Microscope (SEM) in order to identify internal compositional variability and to select homogeneous areas for age determination. U-Pb isotopic analysis was conducted using a New Wave 213 nm Nd-YAG laser coupled to an Agilent 7500cs ICP-MS at the University of Adelaide. Ablation was performed in a helium atmosphere, with a beam diameter of approximately 15 µm at the sample surface, a repetition rate of 5 Hz and laser intensity of 9-10 J cm^{-2}. Each analytical run had a total acquisition time of 100 s, comprising 40 s of background measurement, 10 s of laser firing with the shutter closed to allow for beam stabilisation and 60 s of sample ablation. Isotopic masses were measured for 10 ms, 15 ms, 30 ms and 15 ms for ^{204}Pb, ^{206}Pb, ^{207}Pb and ^{238}U respectively. The comprehensive methodology followed for monazite isotopic analysis is outlined in Payne et al. (2008).

Raw LA–ICP–MS data was processed using ‘GLITTER’, a data reduction program developed at Macquarie University, Sydney (Griffin *et al.* 2008). U-Pb fractionation was corrected for using the internal monazite standard MAdel (TIMS normalisation data: $^{207}Pb/^{206}Pb$ age= 491.0 ± 2.7 Ma; $^{206}Pb/^{238}U$ age= 518.37 ± 0.99 Ma; $^{207}Pb/^{235}U$ age= 513.13 ± 0.19 Ma: (Payne et al. 2008; updated with additional TIMS data)). The accuracy of data

correction was monitored by repeated analysis of the in-house monazite standard 94-222/Bruna NW (*c.* 450 Ma) (Payne *et al.* 2008). Signals were examined carefully for anomalous portions of signal related to zones of Pb loss or gain and the best portion of each ablation signal were selected for age and error determination. Common lead was not corrected for during data reduction; however analyses were discarded if common lead levels, indicated by proxy with the ^{204}Pb isotope, rose to levels high enough to compromise the integrity of the output age. Throughout the study, the weighted averages obtained for MAdel are ^{207}Pb/^{206}Pb= 491.1±5.3 Ma (*n*=144, MSWD=0.93), ^{206}Pb/^{238}U= 518.5±1.2 Ma (*n*=144, MSWD=0.73) and ^{207}Pb/^{235}Pb= 513.3±1.3 Ma (*n*=122, MSWD=0.90), 222 are ^{207}Pb/^{206}Pb= 458.9±9.8 Ma (*n*=48, MSWD=0.91), ^{206}Pb/^{238}U= 453.3±2.8 Ma (*n*=48, MSWD=2.3) and ^{207}Pb/^{235}Pb= 453.3±2.3 Ma (*n*=48, MSWD=1.4).

U-Pb ZIRCON LA–ICP–MS GEOCHRONOLOGY

Zircon grains were separated from crushed rock and mounted in epoxy resin as described for monazite. Sample preparation of stream sediments commenced with sieving as there was no rock to be crushed. Prior to LA–ICP–MS analysis, all zircon grains were imaged using a backscattered electron (BSE) detector and cathodoluminescence (CL) detector on a Phillips XL20 Scanning Electron Microscope (SEM) in order to study their internal structural, determine if multiple age components were present and to select homogeneous areas for age determination.

U-Pb isotopic analyses of zircon grains were obtained using a similar methodology to monazite geochronology. Laser ablation was performed with a beam diameter of approximately 30 μm at the sample surface, a repetition rate of 5 Hz and laser intensity of 9-10 J.cm^{-2}. Each analysis consisted of a total acquisition time of 120 s, comprising of 40 s background measurement, 10 s of laser firing with the shutter closed to allow for beam

stabilisation and 80 s of sample ablation. Isotope masses were measured for 10 ms, 15 ms, 30 ms, 10 ms, 10 ms and 15 ms for ^{204}Pb, ^{206}Pb, ^{207}Pb, ^{208}Pb, ^{232}Th and ^{238}U respectively. U-Pb fractionation was corrected for using the external zircon standard GJ (TIMS normalisation data: $^{207}Pb/^{206}Pb$ age= 607.7 ± 4.3 Ma; $^{206}Pb/^{238}U$ age= 600.7 ± 1.1 Ma; $^{207}Pb/^{235}U$ age= 602.0 ± 1.0 Ma:(Jackson *et al.* 2004)). The accuracy of data correction was monitored by repeated analysis of the internal zircon standard Plešovice (ID-TIMS normalisation data: $^{207}Pb/^{206}Pb$ age= 337.13 ± 0.37 Ma (Sláma *et al.* 2008)). Raw data was reduced using 'GLITTER' and common lead was not corrected for as outlined above for monazite. Throughout the study, the weighted averages obtained for GJ are $^{207}Pb/^{206}Pb$= 608.2±2.7 Ma (*n*=521, MSWD=0.43), $^{206}Pb/^{238}U$= 600.8 ± 0.9 Ma (*n*=521, MSWD=1.6) and $^{207}Pb/^{235}Pb$= 602.2 ±0.8 Ma (*n*=521, MSWD=1.3) and Plešovice are $^{207}Pb/^{206}Pb$= 339.5 ± 4.7 Ma (*n*=169, MSWD=0.67), $^{206}Pb/^{238}U$= 338.3 ± 1.1 Ma (*n*=169, MSWD=2.4) and $^{207}Pb/^{235}Pb$= 338.3 ± 1.0 Ma (*n*=169, MSWD=2.2).

Reduced monazite and zircon data were exported into Excel where subsequent conventional concordia and weighted average plots were generated using Isoplot v4.11 (Ludwig 2003).

APPENDIX D: ZIRCON & MONAZITE GRAIN MORPHOLOGY DESCRIPTION

MONAZITE MORPHOLOGIES

RBN-18

Analysed grains ranged from euhedral to subhedral in shape and ranged in diameter between approximately 80–220 μm. Some monazite grains were fractured and some contained inclusions. Two grains exhibited zoning in BSE imaging, with darker domains occurring at the rims.

RBN-43

Analysed grains were typically anhedral and fractured; grains ranged from rounded to elongate and were blocky, angular and fragmented. Grains analysed ranged in diameter between approximately 25–200 μm and did not exhibit zoning in BSE imaging

RBN-44

Analysed grains were typically subhedral, ranging from rounded to elongate, with some grains slightly fractured and containing inclusions. Grains ranged in diameter between approximately 60–150 μm and exhibited no zoning in BSE imaging.

RBN-54

Grains analysed could be split into two typical morphologies. The first consisted of euhedral to subhedral and possessed spherical shapes, diameters ranging between approximately 80–100 μm and did not exhibit zoning in BSE imaging. The second morphological variety were anhedral to subhedral, highly fractured, 100–200 μm in diameter, contained inclusions under BSE imaging

RBN-61

Analysed grains ranged in diameter between approximately 80–150 μm and did not appear to be zoned in BSE imaging. Grains analysed were typically euhedral to subhedral and possessed spherical shapes.

RBN-67

Grains analysed ranged in diameter between approximately 80–150 μm and did not appear to be zoned in BSE imaging. Analysed grains were typically subhedral and ranged from spherical to elongated.

RBN-68

Concordant grains analysed were typically stubby to spherical and ranged in diameter between approximately 40–110 μm. Few appeared to be zoned in BSE imaging.

RBN-71

Analysed grains ranged in diameter between approximately 80–250 μm and did not appear to be zoned in BSE imaging. Analysed grains were typically euhedral to subhedral and possessed spherical shapes.

ZIRCON MORPHOLOGIES

AS2012-1

Analysed grains were typically elongate, euhedral to subhedral and had mostly rounded edges. Crystals ranged in length between approximately 120–400 μm with aspect ratios of 1:3. Most grains contain fractures and under CL exhibit weak to highly luminescent oscillatory zoning. A proportion of grains exhibit strongly luminescent rims while others exhibit very weakly luminescent rims. Whereas most grains exhibit xenocrystic cores, some exhibit convoluted cores.

AS2012-2

Analysed grains typically varied from rounded to elongate, euhedral to subhedral and had mostly rounded edges. Crystals ranged in length between approximately 80–400 μm with aspect ratios of 1:3. Most grains contain fractures and under CL exhibit weak to highly

luminescent oscillatory zoning. A proportion of grains exhibit strongly luminescent rims while others exhibit very weakly luminescent rims. Most grains exhibit convoluted cores.

HCSS

Detrital zircon grains from the Hamilton Creek Stream sediments (HCSS) display euhedral to subhedral, stubby to elongate and translucent pale pink, brownish yellow, to dark brown crystal morphologies. The fraction of smaller zircon grains are typically 80–200 μm in length, while the larger translucent brown fraction (approximately 30%) ranges in length between 200–400μm. The smaller size fraction has a greater variety in colour – brown to yellow to pink – and typically contained more rounded and stubby grains. At least half the grains were fractured, a small proportion of grains were fragments of a larger grain. Under CL, the larger fraction typically exhibits weak luminescent oscillatory and domain zoning, while the smaller fraction of grains typically exhibits moderately to highly luminescent oscillatory and featureless domain zoning. Some grains exhibit transgressive overgrowths and convoluted metamorphic cores, and a large proportion have dark featureless cores with highly luminescent rims.

RBN-18

Under CL, grains typically exhibit weakly to highly luminescent oscillatory zoning, and weakly luminescent domain zoning. Some grains exhibited transgressive overgrowths and convoluted cores. A significant proportion of larger grains (approximately 200–250 μm in length) exhibit dark, non-luminescent cores and moderately luminescent rims.

RBN-20

Analysed grains are typically stubby to elongate, euhedral to subhedral and have mostly rounded edges. Crystals ranged in length between approximately 80–420 μm. Most grains contain fractures and under CL exhibit weak to highly luminescent oscillatory zoning. Most grains exhibit xenocrystic cores, and some exhibit convoluted cores.

RBN-44

Analysed grains are typically equant to stubby, euhedral to subhedral and have rounded edges. Crystals ranged in length between approximately 80–200 μm. Most grains contain fractures and under CL exhibit weak to moderate luminescence and rare oscillatory zoning. Some grains exhibit convoluted cores.

RBN-54

Analysed grains are typically stubby to elongate, euhedral to subhedral and have rounded edges. Crystals ranged in length between approximately 80–200 μm. Most grains contain fractures and under CL exhibit weakly luminescent, well-defined concentric oscillatory and sector zoning. Some grains exhibit convoluted and xenocrystic cores.

RBN-57

Analysed grains are typically stubby to elongate, euhedral to subhedral and have rounded edges. Crystals ranged in length between approximately 100–250 μm. Most grains are fractured and under CL exhibit weakly luminescent, well-defined concentric oscillatory and sector zoning. Some grains exhibit convoluted and/or metamict cores.

RBN-61

Analysed grains are typically stubby to elongate, euhedral to anhedral and have rounded edges. Crystals ranged in length between approximately 80–400 μm. Most grains are highly fractured and under CL exhibit weakly luminescent, poorly-defined concentric oscillatory and sector zoning. Some grains exhibit convoluted and/or metamict cores, and local recrystallization.

RBN-67

Analysed grains are typically stubby to elongate, euhedral to subhedral and have rounded edges. Crystals ranged in length between approximately 100–250 μm. Most grains are fractured and under CL exhibit weakly luminescent, poorly-defined concentric oscillatory

and sector zoning. Some grains exhibit convoluted and/or metamict cores, and local recrystallisation.

RBN-68

Analysed grains are typically stubby to elongate, euhedral to subhedral and have rounded edges. Crystals ranged in length between approximately 100–250 μm. Most grains are fractured and under CL exhibit weakly luminescent, well-defined concentric oscillatory and sector zoning. Some grains exhibit convoluted and/or metamict cores.

RBN-71

Analysed grains are typically stubby to elongate, euhedral to subhedral and have rounded edges. Crystals ranged in length between approximately 100–250 μm. Most grains are fractured and under CL exhibit weakly luminescent, poorly-defined concentric oscillatory and sector zoning. Some grains exhibit convoluted and/or metamict cores, and local recrystallisation.

APPENDIX E: U-Pb MONAZITE LA-ICP-MS DATA

Separate document.

APPENDIX F: U-Pb ZIRCON LA-ICP-MS DATA

Separate document.